Hydrogen transport in nickel (111)

Roi Baer
Department of Physical Chemistry and the Fritz Haber Research Center, The Hebrew University, Jerusalem 91904, Israel

Yehuda Zeiri
Department of Chemistry, Nuclear Research Center-Negev, Beer-Sheva 84190, P.O. Box 9001, Israel

Ronnie Kosloff
Department of Physical Chemistry and the Fritz Haber Research Center, The Hebrew University, Jerusalem 91904, Israel
(Received 13 November 1996; revised manuscript received 21 January 1997)

The intricate dynamics of hydrogen on a nickel (111) surface is investigated. The purpose is to understand the unique recombination reaction of subsurface with surface hydrogen on the nickel host. The analysis is based on the embedded diatomics in molecules many-body potential surface. This potential enables a consistent evaluation of different hydrogen pathways in the nickel host. It is found that the pathway to subsurface-surface hydrogen recombination involves crossing a potential-energy barrier. Due to the light mass of the hydrogen the primary reaction route at low temperature occurs via tunneling. A critical evaluation of tunneling dynamics in a many-body environment has been carried out, based on a fully quantum description. The activated transport of subsurface hydrogen to a surface site, the resurfacing event, has been studied in detail. It is shown that the tunneling dynamics is dominated by correlated motion of the hydrogen and the nickel hosts. A fully correlated quantum-dynamical description in a multimode environment was constructed and employed. The ''surrogate Hamiltonian method'' represents the nickel host effect on the hydrogen dynamics as that of a set of two-level systems. The spectral density, which is the input of the theory is obtained via classical molecular-dynamics simulations. The analysis then shows that the environment can both promote and hinder the tunneling rate by orders of magnitude. Specifically for hydrogen in the nickel host, the net effect is suppression of tunneling compared to a frozen lattice approximation. The added effect of nonadiabatic interactions with the electron-hole pairs on the hydrogen tunneling rate was studied by an appropriate ''surrogate Hamiltonian'' with the result of a small suppression depending on the electron density of nickel. The resurfacing rates together with surface recombination rates and relaxation rates were incorporated in a kinetic model describing thermal-desorption spectra. Conditions for a thermal-programmed-desorption peak which manifest the subsurface-surface hydrogen recombination were found. [S0163-1829(97)09216-3]

I. INTRODUCTION

Hydrogen has a strong affinity for nickel, leading to the use of nickel as a heterogeneous catalyst for hydrogenation reactions. When a hydrogen molecule approaches the nickel surface it readily dissociates and adsorbs.[1] When atomic hydrogen approaches the surface it primarily adsorbs on the surfaces, but a minority is absorbed into the crystal bulk.[2,3] Once adsorbed or absorbed, the hydrogen may wander on the crystal surface[4–6] or plunge into the bulk. This motion involves crossing potential-energy barriers which separate the various interstitial and adsorption sites. Thus hydrogen motion in nickel involves activated transport which, at low temperatures, is controlled predominantly by tunneling.[7,8]

When a cold nickel crystal containing hydrogen is heated, molecular hydrogen is ejected into the gas phase.[2,3,9,10] For nickel crystals which have been exposed to molecular hydrogen, recombinative desorption takes place at high temperatures, peaking at 350 K. However, for crystals which have been exposed to atomic hydrogen, a recombination is observed at lower temperatures of 180–200 K, in addition to the peak at 350 K. These findings suggest that low-temperature desorption is due to a recombination of subsurface and surface atomic hydrogen species.

The present study was initially aimed at elucidating the dynamics involved in surface-subsurface hydrogen recombination, and to seek theoretical support for this special hydrogenation mechanism.[10] It was soon appreciated that unraveling the reaction mechanism would require a complete assessment of a variety of hydrogen dynamical processes in the nickel host. The light mass of hydrogen emphasizes quantum effects. The dominant phenomenon is tunneling. To gain insight into the process, a critical evaluation of theoretical approaches to many-body tunneling phenomena is required. The failure of simple approximations has led to the development of theoretical tools for the assessment of tunneling in dissipative environments. The odyssey of the present study finally returned to the original problem of subsurface-surface recombination, indicating the conditions which enable the existence of such a process.

Previous theoretical efforts for hydrogen on nickel have focused primarily on determining the adsorption probabilities on a frozen crystal.[11,12] Theoretical treatments of other hydrogen-metal interactions have also concentrated on adsorption, the assumption being that detailed balance can explain the experimental desorption results.[13–16] This approach can, in principle, yield desorption-product state distributions when the multimode character of the metal host is not

coupled to the reaction transition state. This is probably the case for the H_2/Cu system.[17,18] However, for recombination of a subsurface hydrogen with a surface hydrogen, the reaction transition state is strongly influenced by the motion of the metal atoms, and detailed balance considerations cannot yield a simple description.

Most of the theoretical effort has been devoted to H_2/Cu adsorption, which has become the benchmark system for activated gas-surface dynamics. Detailed and accurate adsorption/desorption experiments, performed by Rettner, Michelsen, and Auerbach[19,20] for H_2/Cu, have stimulated extensive theoretical work.[21,22] A few of the experimental features are understood, among them vibrational-assisted sticking and rotational effects. These studies show that the dynamics of adsorption, even with a few degrees of freedom, is complex, where steering effects and barrier locations have a strong impact on the dynamical behavior.

The benchmark system for nonactivated adsorption is the hydrogen/Pd system, for which adsorption probabilities were calculated by Gross[23] for the six degrees of freedom of the two hydrogen atoms. This work showed that surface corrugation has a role in determining adsorption probabilities. Desorption state distributions were calculated by Gross for the experimental temperature.

One of the important conclusions from the various theoretical investigations is that reduced dimensionality treatments predict higher probabilities compared to those of full dimensionality, for example, the resurfacing of bulk hydrogen defined as the transport from a subsurface to a surface site.[8] In this case the reaction-path one-dimensional (1D) rates differed by two orders of magnitude from the full 3D rates. This is due to the extreme sensitivity of the tunneling process to any feature of the system. A similar discrepancy, between 2D and 3D results, is observed for Pd surface penetration by atomic hydrogen.[24] Sticking probabilities also exhibit a large sensitivity to reduced dimensionality.[22]

The system under study is the low-temperature dynamics of hydrogen within the metal bulk and on its surface. The difficulty in setting up a dynamical framework for the involved processes stems from the combination of the many-body aspect of the interactions, and from the quantum nature of hydrogen dynamics at low temperatures. Though direct calculations of up to six dimensions are possible,[23] they are not sufficient to capture the role of other degrees of freedom in the system. Two types of many-body effects need to be addressed: First, the interaction of an adsorbate with the phonon modes of the crystal motion, and second, the nonadiabatic interaction with the conduction electrons of the metal.

Vibrational line shapes of adsorbed hydrogen, originating from nonadiabatic interactions, have been investigated by Persson and Hellsing.[25,26] For heavier molecular species, such as CO on Cu, the nonadiabatic and phononic line broadenings were addressed by Head-Gordon and Tully,[27,28] using molecular-orbital theory and classical dynamics.

Hydrogen diffusion on metals influenced by many-body forces has been studied by the canonical variational transition-state theory with small curvature tunneling correction.[29,7,30] These approaches are reasonably adequate for overbarrier diffusion. For low temperatures the quality of the approximation depends on the validity of the neglected nonadiabatic curvature couplings. The present work develops an approach to the problem of diffusion in metals. One of its benefits is that it is fully quantum mechanical. The approximations used by this method are different than those used by the small curvature reaction path methods.[31]

Explicit multimode bath dynamics is also treated using path-integral approaches.[32] Recently, direct real-time path-integral approaches[33,34] have been developed, but these have not yet been used for analyzing atomic diffusion on metals. Path centroid transition state methods[35–37] supplemented by molecular-dynamics simulations[38–42] were recently used for assessing the low-temperature diffusion rates of atomic hydrogen on nickel. Such indirect schemes are complementary to the direct propagation method employed here. For diffusion in a perfectly periodic environment a direct band motion analysis has been employed.[43–45] However, for the temperatures addressed here, such a treatment is inadequate, due to the destruction of coherent tunneling caused by crystal vibrations and nonadiabatic interactions.[46,47]

Energy loss to phonons in gas-surface scattering, and its assistance to sticking, has also received much attention. Most studies have employed classical dynamics,[48,49] which is suitable for heavier elements than hydrogen.[50,51] Some semiclassical methods[52,53] and quantum-classical treatments[54–56] have also been used. A pure quantal calculation for inelastic energy transfer and sticking probabilities was developed by Stiles, Wilkins, and Persson[57] and Jackson.[58] The approach is based on a one-phonon model, suited for direct, short-time interactions, where the simultaneous excitation of several phonon modes may be neglected.

The tour through the different approaches to hydrogen-metal encounters eventually has to return to the original problem. The unique subsurface-surface reaction mechanism amounts to a direct encounter between bulk hydrogen and surface hydrogen atoms steered by the nickel atoms. It seems that only such a mechanism is able to explain the low temperature peak in the thermal-programmed-absorption (TPD) experiments. A dynamical model able to explain these results has to include explicitly dynamics lattice.

The rate-limiting step in such a model is the transport of the subsurface hydrogen to the metal surface which will be termed resurfacing. It is known from experiment that hydrogen contained in a cold metal resurfaces on a time scale of hours.[59] This is in contrast to the resurfacing time calculated by using a frozen lattice which employed the embedded atom potential[60] (EAM), found to be of the order of seconds.[8] The discrepancy between the experiment and the calculation of 2–3 orders of magnitude suggest that either the barrier structure predicted by the EAM is wrong, or that resurfacing rates are highly affected by either nonadiabatic effects or the crystal motion or by both. As will be shown in this study, the dissipative forces indeed are strong enough to explain the discrepancy.

The most obvious role of the phonon motion is its influence on the barrier height and width. The motion enhances the tunneling, and is known as phonon-assisted diffusion. Such an effect can naturally be taken into account by a sudden approximation, exploiting the nickel-hydrogen large mass ratio. It will be shown that the simplest approach of adiabatic separation leads to gross errors in estimating the tunneling rates.

The phonon motion can also induce a loss of coherence

which acts to deplete the tunneling rates.[32] The relative importance of phonon assistance and hindrance must be ascertained quantitatively. In this study the surrogate Hamiltonian method is used to treat the many-body effects,[61] see Appendix A for a short description. Approximately three different ''phonon baths'' are necessary to define the interaction with the resurfacing hydrogen atom. The combined effect of these baths reduces the tunneling rate by as much as two orders of magnitude.

The surrogate Hamiltonian is also employed to study the non-adiabatic electron-hole pair excitations. For this specific system the reduction of the tunneling rate is small.

The final process analyzed separately is the recombination of two hydrogen atoms leading to H_2 desorption. Only a limited study is possible due to the high dimensionality of the process. The temperature dependence of the tunneling rates shows a universal character where, at low temperature, the rate is temperature independent, and where, above a crossover temperature, it changes to an Ahrenius relation.

Finally all these processes are combined in a kinetic model simulating the temperature program desorption experiments. Qualitative conditions where the subsurface hydrogen recombines with a surface hydrogen at lower temperature than two surface hydrogen can be found.

II. POTENTIAL ENERGY OF THE H/NI(111) SYSTEM

In the intricate dynamics of hydrogen with a nickel crystal, the potential-energy surface plays a key role. The potential-energy surface is the basic entity from which the forces are derived in a molecular-dynamics (MD) simulation. It also governs the wave-function dynamics in a quantum calculation. The main difficulty for the MD simulation task is the large number of participating atoms which require a calculation of the forces for all atoms. This means that computations of large systems are possible only if the evaluation of the potential-energy surface (PES) is simple and economic.

Over a decade ago, Daw and Baskes[60] proposed an approach, the EAM, for calculating the PES of hydrogen interacting with transition metal surfaces (i.e., Ni and Pd). The EAM is a semiempirical method based on the density-functional theory.[62] In the EAM, the total energy of the system is described by

$$E=\sum_i F_i(\rho(h,i))+\frac{1}{2}\sum_{i\neq j}\phi_{ij}(R(i,j)), \qquad (2.1)$$

where $F_i(\rho(h,i))$ is the embedding function of atom i in the electron density of the neighboring atoms $\rho(h,i)$, and $\phi_{i,j}$ is a pairwise electrostatic repulsion term which is cast into an analytic function characterized by a number of parameters. These parameters, together with the embedding functions, are determined semiempirically by requiring that characteristics of the solid-hydrogen system be reproduced by the EAM potential. The quantities used are lattice constant, elastic constants, sublimation energy, vacancy formation energy, and the energy difference between the bcc and fcc phases. The EAM results in a very close agreement between the calculated and experimental values for H/Ni and H/Pd systems. In addition to its accuracy, the EAM is especially suited for MD simulations since calculation of the forces requires only a small additional effort to the calculation of the potential.

More recently, Truong, Truhlar, and Garrett[63] developed a similar approach termed ''embedded diatomics in molecules'' (EDIM). The approach was used for the investigation of single, two, and three hydrogen atoms interacting with a nickel surface. The agreement between these calculations and other theoretical as well as experimental studies was very satisfactory. For a single hydrogen interacting with the metal surface, the EDIM is similar to the EAM. There are a number of differences related to the functional form of the electrostatic repulsion terms. Moreover, in the EDIM approach there is a distinction between the screening constants used in the calculation of electron orbitals located on surface and bulk atoms. For a larger number of hydrogen atoms, PES's are calculated by the diatomics in molecule formalism where the H-surface ground and excited potential are calculated by using an EAM-type procedure (as for a single H atom).

In the present study, the EDIM approach was adopted. It was used to evaluate the interaction potentials in all the classical- and quantum-mechanical studies described below. The parameters were adopted from Ref. 63. The potential along a cut leading from the subsurface to surface site was compared to an *ab initio* calculation based on a Gaussian DFT method. The differences were less than 0.02 eV. The potential is designed to give the correct asymptotic description of the H_2 molecule. In the following two subsections a brief description of the the H/Ni(111) and H_2/Ni(111) potential-energy surfaces will be discussed.

A. PES for a single hydrogen atom near Ni(111)

The Ni(111) surface exhibits four high symmetry adsorption sites: on-top, bridge, and two threefold sites. These threefold sites differ by the position of the second-layer nickel atoms. The fcc threefold site has a nickel atom right below it, while the hcp threefold site (also termed threefold hollow site) has a nickel atom only in the third layer (Fig. 1).

The EAM and EDIM (Refs. 60 and 63) calculations showed, in agreement with experimental results, that the largest H/Ni(111) binding is obtained for the threefold hollow (hcp) site. The differences between the binding of the hydrogen to this site and the other high-symmetry sites was quite small (in the range of 0.03–0.3 kcal/mole). Larger differences were obtained for the vibrational frequencies associated with these four adsorption sites.

The present study focuses on the dynamics associated with the emergence of subsurface hydrogen onto the metal surface (a phenomenon termed ''resurfacing''). A cut of the PES of a hydrogen atom in a plane normal to the surface and along one of the parallel directions is shown in Fig. 2. Here the negative-Z values correspond to the subsurface positions of the hydrogen atom. As can be seen in the figures, the most stable subsurface site for hydrogen is 1 Å below the threefold hollow site. The binding energy at this octahedral subsurface site is approximately 0.5 eV smaller than at the threefold hollow site on the surface (see the inset in Fig. 2). Thus the subsurface sites are metastable potential-energy wells. When the zero point energies are taken into account this difference increases.

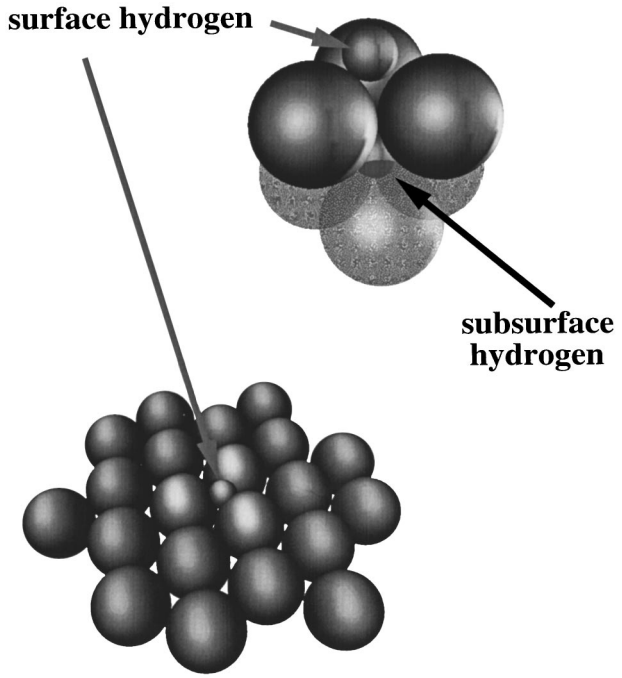

FIG. 1. The Ni(111) surface and the positions of the hydrogen atom. The surface hydrogen in the picture is located in a threefold hollow (hcp site).

There exist other subsurface (bulk) sites for the hydrogen atom, the one below the threefold fcc surface site being an example. However, the octahedral subsurface site is the most stable position for the H atom below the surface and in the bulk. This agrees well with the experimental data and with other calculations.[2,10,3]

Inspection of the PES in Fig. 2 shows that the subsurface hydrogen at the octahedral site can resurface by following two main paths. One is the direct pathway leading upwards to the threefold hollow site, and the other is via a neighboring tetrahedral subsurface site, which finally surfaces at the threefold fcc site. Along the first route, the H atom has to overcome an energy barrier of approximately 0.6 eV. On the second path the energy barrier is approximately 1.6 eV. Such a large difference in barrier heights suggests that the only practical way for the hydrogen to resurface is via the direct route leading from the octahedral to the threefold hollow site.

The thermal motion of the lattice atoms may result in a slight ''opening'' of the hexagonal structure, which temporarily lowers the energy barrier for the surfacing motion. This possibility is shown in Fig. 3, where a cut of the minimal potential-energy path along the perpendicular Z direction is shown. When the surface Ni-atom triad are symmetrically displaced, increasing their mutual separation, the barrier for hydrogen surfacing is significantly reduced. Note that the stability of the metastable potential well is also increased as a result of this motion. These energetical aspects of the lattice motion will be addressed in the sections concerning the hydrogen atom dynamics (see Secs. V and VI).

B. PES of the interaction between two hydrogen atoms and Ni(111)

The binding energy of two hydrogen atoms to two neighboring threefold sites on the surface is approximately 2.6 eV per H atom. Hence, in the event of recombinative desorption of two hydrogen atoms, 5.2 eV of energy has to be supplied to break the H-surface bonds, while only about 4.7 eV are gained in the creation of the H_2 bond. As a result, the desorption process is endothermic by approximately 0.5 eV. A cut in the six-dimensional PES describing a recombinative desorption process of two surface hydrogen atoms is shown in Fig. 4.

In Fig. 4 the PES as a function of the H-H separation r and the H_2 center-of-mass–surface-normal distance Z are

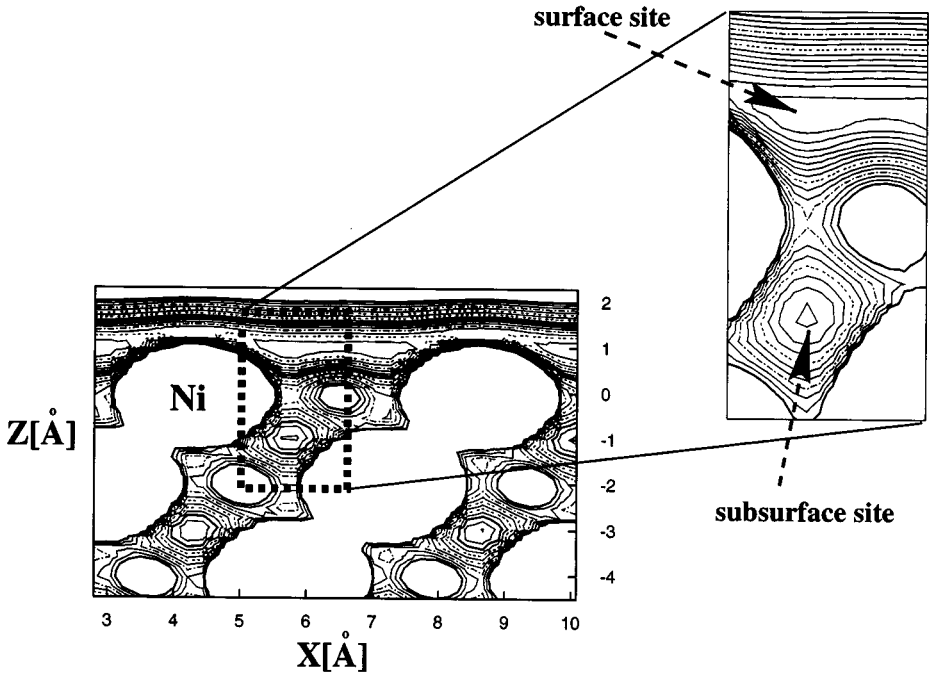

FIG. 2. The EDIM-based potential energy surface of hydrogen in nickel as a function of the distance from the metal surface (Z) and parallel to the surface coordinate (X). The low potential passageways intertwining among high-potential-energy mountains of the metal atom cores are clearly observed. The inset focuses on the most stable subsurface site, the threefold octahedral site, which is metastable with respect to the surface binding hcp and fcc binding sites. The H atom tunnels from it to the surface through a potential-energy barrier. The potential difference between two adjacent contour lines in the figure is 0.1 eV.

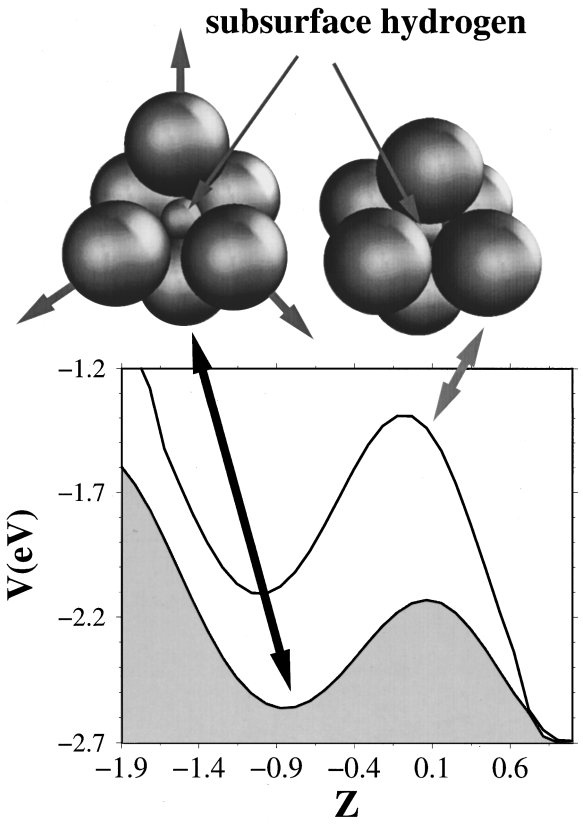

FIG. 3. Top: Views of the nickel atoms at their lattice points (right) and of an open nickel triangle (left). Below: The corresponding reaction path potentials for hydrogen. These paths have been adiabatically corrected for the perpendicular mode zero-point energies. The open configuration was obtained from a MD simulation at 90 K corresponding to the lowest barrier in a 10-ps simulation period.

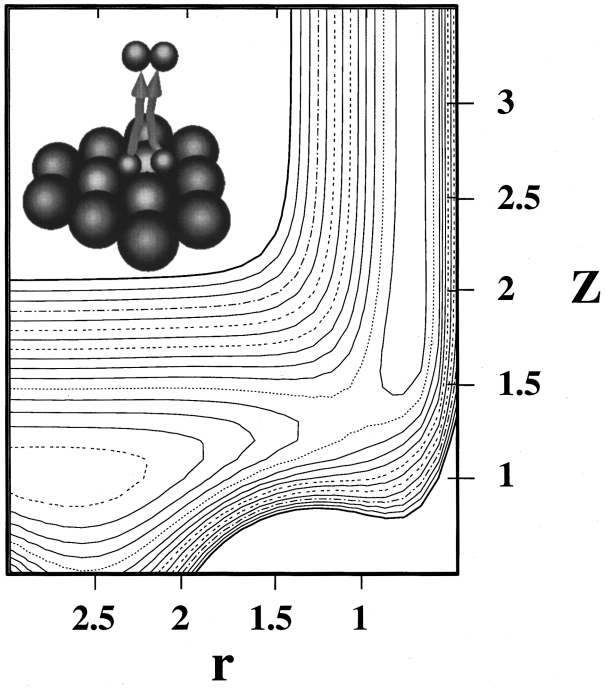

FIG. 4. A two-dimensional potential-energy surface contour map for the recombination of two surface hydrogen atoms. The nuclear separation between hydrogens is r (Å), and the center of mass distance from the nickel surface is Z (Å). A flat orientational angle of the H-H axis from the surface has been chosen. The double adsorption well of the two hydrogen atoms is 5.2 eV deep. The reaction path leads to the H_2 molecular well 4.72 eV in depth. Transversing a sketchy reaction path, the system encounters a high potential barrier, and exhibits an overall desorption endothermicity. This explains the high-temperature needed to desorb surface hydrogen in a TPD experiment ($\sim$350 K). The potential difference between adjacent contour lines is 0.2 eV.

shown. The endothermicity of the desorption process, as well as a potential barrier for adsorption of 0.17 eV along the reaction path, can be clearly seen. These two factors explain the relatively high temperature (350 K) needed to desorb hydrogen from a Ni(111) surface. It should be noted that the Ni(111) surface is quite flat; hence the energy barriers associated with surface diffusion between adjacent sites are small.

When subsurface hydrogen is present in the metal, there arises another route for hydrogen recombination: a reaction among surface and subsurface hydrogen atoms. This possibility was conjectured by Johnson *et al.*[2] after observing, in the presence of subsurface hydrogen, a TPD peak at 180 K. This lowering of the desorption temperature can be explained by the fact that subsurface hydrogen is less stable than surface hydrogen by about 0.6 eV (including the perpendicular mode zero-point energies), thus reducing or eliminating completely the endothermicity of the reaction. However, the reaction must be direct to prevent quenching by dissipative effects. Therefore, the two hydrogen atoms must be neighbors.

One case that deserves attention is the nearest neighbor reaction, where the surface atom is situated in the threefold hollow site directly above the subsurface hydrogen atom. A cut of the potential-energy surface for this type of reaction is shown in Fig. 5. It is seen that this reaction is possible only by the crossing of a 1.2-eV potential barrier. This high barrier is expected to yield a high recombination temperature, and, therefore, this pathway can be discarded when considering the temperature decrease in the TPD peak due to subsurface hydrogen.

The other possible reaction path of subsurface-surface recombination reaction involves a surface hydrogen atom initially located in the nearest threefold fcc site. The energetics of this reaction are demonstrated by using a sequence of four cuts of the potential-energy surface, as shown in Fig. 6.

The PES cuts in Fig. 6 represent the variation of energy as a function of the H-H separation in a direction parallel to the surface and the position of the subsurface hydrogen along the surface normal Z_2. Negative values of Z represent subsurface positions. Each of the four cuts corresponds to a different height of the surface H above the surface plane ($Z_1 = 0.7$, 0.9, 1.1, and 1.7 Å). These results clearly show that the reaction path is curved, with a desorption barrier of approximately 0.65 eV. As will be shown in the next sections, significant tunneling rates of subsurface hydrogen can be achieved at the experimental desorption TPD temperatures.

The relative magnitudes of the energy barriers for desorption along these two pathways suggest that the dominant route is the second one. Moreover, the occupation of the threefold hollow sites on the surface by adsorbed hydrogens

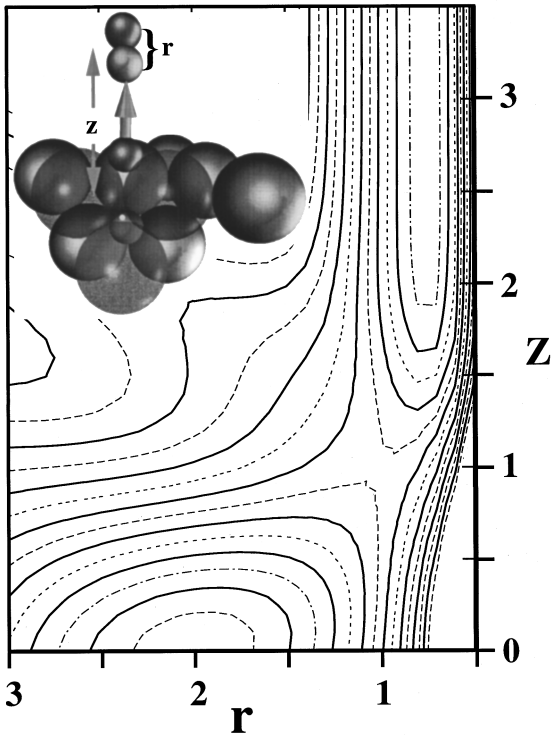

FIG. 5. A two-dimensional potential-energy surface contour map of the recombination of a subsurface hydrogen (octahedral site) with a surface hydrogen atom at a threefold hollow site. The nuclear separation between hydrogens is r Å and the center of mass distance from the nickel surface is Z Å. The H-H axis is perpendicular to the surface in this cut. The potential difference between adjacent contour lines is 0.2 eV.

prevents the emergence of subsurface H through the octahedral site onto the surface. Thus the surface hydrogen at the hcp sites serves as a cap to the resurfacing process. Further discussion of the dynamics associated with this desorption process will be presented in subsequent sections.

III. MOLECULAR-DYNAMICS SIMULATIONS

Insight into the intricate dynamics of hydrogen in the nickel crystal is gained by molecular-dynamics simulation. However, the MD simulations cannot by themselves describe the complete story of hydrogen resurfacing and recombination. The phenomenon is a low-temperature one and, due to hydrogen tunneling, requires a quantum-description. Yet a quantum-mechanical calculation becomes prohibitively expensive when the many-body aspect of the crystal motion coupled to the quantum tunneling is considered. Therefore, a combined strategy is used in which information gained from the classical MD simulation is incorporated into a reduced dimensional quantum calculation, as will be described in Secs. V and VI. Tunneling rates are exponentially sensitive to the potential barrier height, which is determined by the positions of the adjacent nickel atoms. Thus, for calculating the resurfacing rates, it is essential to determine the distribution of barrier heights during the thermal motion of the crystal. The results of such a simulation are shown in Secs. V A and VI.

A. Molecular-dynamics setup

In all MD simulations described in this study, the nickel solid is represented by a slab of six movable layers, 24 atoms

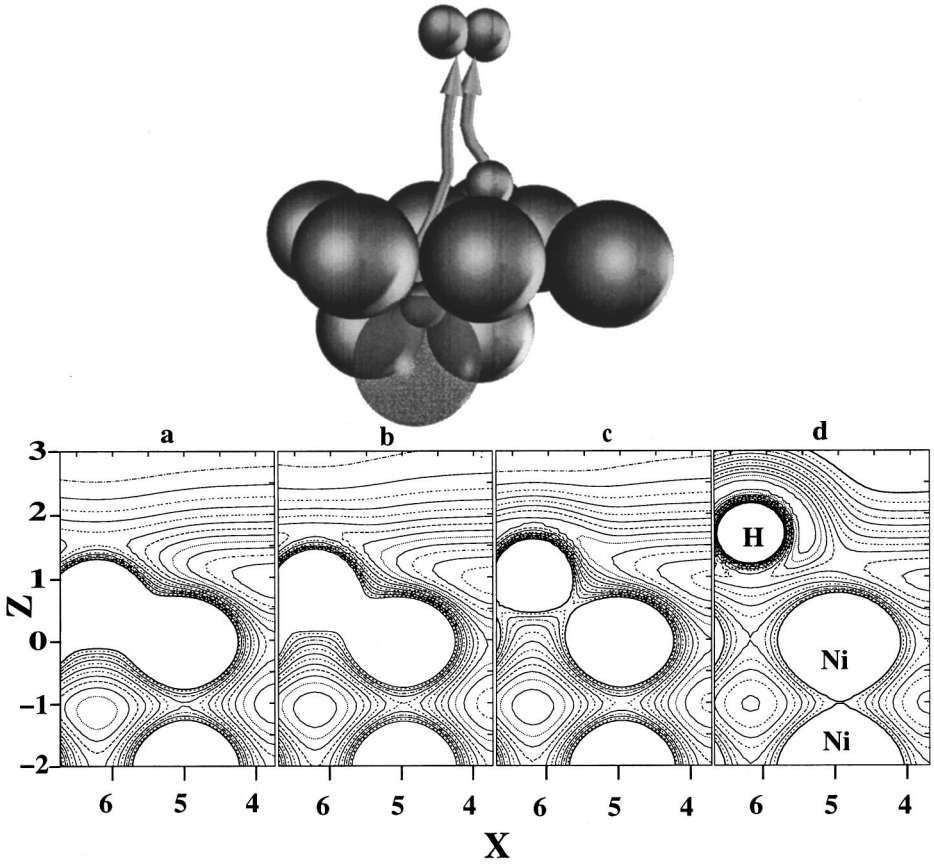

FIG. 6. A sequence of two-dimensional potential-energy surfaces for the recombination of surface and subsurface hydrogen atoms. The surface hydrogen atom position Z_1 is fixed at (a) 0.7 Å, (b) 0.9 Å, (c) 1.1 Å, and (d) 1.7 Å, above a fcc threefold surface site. The lateral nuclear coordinate of the second (originally subsurface) H atom is X, and its distance from the nickel surface is Z_2. Notice in (d) the appearance of the H_2 potential-energy well. The potential difference between adjacent contour lines is 0.1 eV.

each, together with two identical but fixed layers, which are situated below the six mobile layers. Periodic boundary conditions were imposed along the directions parallel to the surface. This slab, representing the solid surface, was attached at the bottom layer to 24 fictitious particles representing the heat dissipation into the rest of the solid. The motion of the fictitious particles was governed by a Langevin equation.[64,65,48,66,67] Integration was performed by a third-order predictor corrector method,[68] using 1-fs time steps. Such a short time step was required in the hydrogen penetration calculation because of the large accelerations of the H atom as it approaches the solid surface from the gas phase.

B. Hydrogen-atom penetration into the solid

One of the experimental procedures to introduce hydrogen into the bulk metal is by exposing the crystal to a flux of hydrogen atoms.[2,10,3] The process was simulated by MD calculations with the purpose of examining its efficiency. The initial conditions for the simulations sampled thermal hydrogen atoms moving toward a threefold hollow or toward a threefold fcc site on the surface. In each simulation 250 trajectories were calculated where the termination conditions were as follows: (1) the hydrogen atom was inside the solid, with a kinetic energy of less than 0.5 eV; (2) the hydrogen atom was above the surface, with a kinetic energy of less than 0.7 eV; (3) the hydrogen atom was scattered back to the gas phase; and (4) the trajectory time exceeded 25 000 integration steps (25 ps).

Conditions (1) and (2) above correspond to bulk and surface hydrogens, respectively. Universally in all trajectories calculated, the hydrogen atom is captured by the metal phase. As the hydrogen atom approaches the solid, it becomes accelerated by its strong attraction to the surface. The translational energy gained by this acceleration ($\sim$2.6 eV) allows the hydrogen to cross the energy barrier between the surface and bulk ($\sim$0.9 eV) easily. After the hydrogen atom penetrates the solid it executes a large number of collisions with the Ni atoms before it reaches termination conditions. The large difference between masses of hydrogen and nickel restrict energy transfer from the hydrogen atom to the bulk.

Four sets of calculations were performed in which the target site on the surface and the incidence angle θ (polar angle) of the hydrogen were varied. The probability of the hydrogen atom penetrating the solid and remaining in the bulk, Prob(in), was found to be independent of the target site on the surface. The probability of forming subsurface and bulk hydrogen was 0.43 for the threefold hollow and 0.42 for the threefold fcc. In addition, a very weak dependence of these probabilities on the incidence angle θ(in) was found. The change of θ from 0° to 30° yielded penetration probabilities of 0.45 and 0.43 for the two target sites, respectively. These changes in Prob(in) are smaller than the error in the simulations, hence Prob(in) is practically independent of θ. The conclusion from these simulations is that Prob(in) is relatively insensitive to the nature of the target site and the incident angle θ of the H atom. Since none of the hydrogen atoms were scattered back to the gas phase, the probabilities for finding the hydrogen adsorbed to the nickel surface are given by the fraction needed to complete the above probabilities to unity.

Inspection of the time evolution of the actual trajectories shows that the hydrogen atom always penetrates into the subsurface region. The rate of energy loss is very slow due to the mass mismatch, and, therefore, the hydrogen atom undergoes many collisions before it comes to rest in a locally stable site. This site may be either on the surface or in the bulk. It should be noted that most of the trajectories were terminated due to the fourth termination condition. Thus the values of Prob(in) presented above serve only as upper limits for the bulk hydrogen formation probability. The order-of-magnitude discrepancy between the calculated and measured[2] Prob(in) values indicates that a large fraction of the hydrogen atoms defined in the simulation as bulk hydrogen will emerge on the surface at later times. In addition, the accumulation of bulk hydrogen may also result in a reduction of Prob(in) values due to a blockage of the pathway for further hydrogen penetration. This effect was not examined in the present calculations. In the simulations described above the only dissipation mechanism considered was energy loss to the phonon bath of the solid.

Another possible route of energy dissipation is the excitation of metal electrons. To examine the importance of this channel of energy loss, additional calculations were performed in which electronic friction and the corresponding random force were included in the hydrogen equations of motion. The electronic friction was computed according to the method of Li and Wahnstrom.[38,42]

The probability of forming subsurface and bulk hydrogen for the two types of target surface sites was found to be 0.54 for the threefold hollow site, and 0.31 for the threefold fcc site. These results show quite a different behavior than those described above. For the threefold hollow site, Prob(in) increased by about 25%, indicating that the more efficient energy loss of the penetrating hydrogen atom results in an increase of subsurface (bulk) population. On the other hand, for the threefold fcc site a large reduction in the probability of forming bulk hydrogen was observed. This marked decrease in the magnitude of Prob(in) for this site is due to the large frictional forces induced on the penetrating hydrogen atom during its passage through the high electron density regions near the subsurface Ni atom.

We conclude by emphasizing the importance of electronic excitations during the penetration of hydrogen into a metal. For the relatively high kinetic energies involved, the rate of energy dissipation is linear with the hydrogen kinetic energy.[69,70] As a result, the electrons are able to dissipate energy of fast penetrating hydrogen effectively, causing trapping. The influence of electronic friction on the tunneling motion will be considered in Sec. VII.

IV. RESURFACING DYNAMICS I: ADIABATIC HYDROGEN TUNNELING IN A FROZEN NICKEL LATTICE

By examining the potential-energy surface, it becomes obvious that the resurfacing, and therefore the recombinative reaction, involves tunneling. Specifically the tunneling route is of a hydrogen atom from an hcp subsurface site to the surface. It is well established that tunneling is extremely sensitive to almost any parameter of the system, and hence requires a very careful analysis. The first step in such an analy-

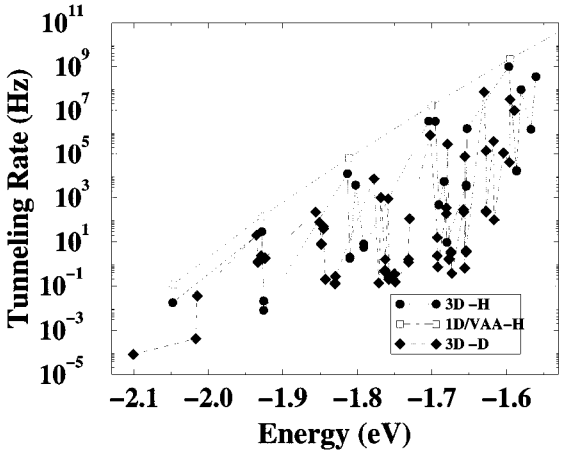

FIG. 7. Tunneling spectrum of subsurface hydrogen and deuterium moving to a surface hcp site for a frozen lattice. Also shown is the 1D VAA approximation for hydrogen.

sis is to construct a reliable numerical procedure which allows accurate calculations for extremely small tunneling rates. It is instructive to write the full Hamiltonian of the problem as

$$\hat{\mathbf{H}}=\hat{\mathbf{H}}_s+\hat{\mathbf{H}}_p+\hat{\mathbf{H}}_e+\hat{\mathbf{V}}_{sp}+\hat{\mathbf{V}}_{se}, \tag{4.1}$$

where $\hat{\mathbf{H}}_s$ is the adiabatic Hamiltonian of the hydrogen. Assuming a frozen lattice, $\hat{\mathbf{H}}_p$ is the lattice Hamiltonian, composed of the nickel vibrational modes, and $\hat{\mathbf{H}}_e$ is the Hamiltonian of the conduction electrons of the metal. The lattice and conduction electron Hamiltonians, are both coupled to the hydrogen motion by the potentials $\hat{\mathbf{V}}_{sp}$ and $\hat{\mathbf{V}}_{se}$.

The problem of the hydrogen resurfacing rate is first analyzed by assuming a frozen lattice, and assuming that the dynamics is electronically adiabatic: $\hat{\mathbf{V}}_{sp}=\hat{\mathbf{V}}_{se}=0$. This analysis constitutes a reference for further calculations where these couplings are taken into account (Secs. V, VI, and VII).

The principal problem in calculating tunneling rates is the experimental time scale of the order of seconds compared to the basic vibrational subpicoseconds time scale. This fact imposes an extreme accuracy requirement on the tunneling rate computation. The method developed for the purpose has an accuracy spanning 14 orders of magnitude. The method is based on a Fourier grid representation of the wave functions. A time-energy filter extracts the individual tunneling eigenstates from the metastable well eigenstates, acting as initial guesses. Outgoing boundary conditions are imposed by the use of imaginary potentials localized in the asymptotes. Details of the method are described in Ref. 8. A typical tunneling spectrum, showing the lifetime of the tunneling states as a function of energy for resurfacing of hydrogen and deuterium, is shown in Fig. 7.

Two points should be emphasized. There is a finite tunneling rate from the ground state, meaning that the subsurface site is metastable, stabilized only when all surface sites are occupied. The other point is that, for each temperature, the tunneling rate is determined by very few eigenstates representing the balance between exponential increase of the tunneling rate with energy and exponential decrease due to Boltzmann weighting. This fact has also been pointed out by Wonchoba, Hu, and Truhlar.[7] Comparing hydrogen to deuterium in Fig. 7, it is observed that the tunneling from the ground state of deuterium is two orders of magnitude lower than for hydrogen, and that the density of tunneling states is higher.

The validity of the reduced dimensionality approximation for the tunneling rates was checked in Ref. 8. It was found that these approximations overestimate the tunneling rate by orders of magnitude. The best of the examined approximations was found to be the vibrationally adiabatic approximation (VAA), which overestimates the tunneling rate for low temperatures by a factor of 5. These deficiencies should be taken into consideration when the influence of other effects on the tunneling rates are evaluated.

V. RESURFACING DYNAMICS II: PHONON-ASSISTED TUNNELING

Lattice motion has a profound influence on the tunneling dynamics. In the following sections an incremental analysis is performed, starting from a simple model in this section, which will be elaborated upon in the next sections.

Hydrogen tunneling rates are exponentially sensitive to barrier height and shape. The analysis in Secs. II and III showed that the lattice modes can lower the barrier by opening the nickel-surface-atom triad on the H-atom tunneling route (see Fig. 3).

Simple approximations which includes this effect are desirable. An elementary model consists of a single oscillator representing the thermal bath and its coupling to the barrier dynamics. A further adiabatic simplification has been attempted, based on the favorable mass ratio between the hydrogen and nickel atoms. The adequacy of the model and the adiabatic approximation are assessed in the following subsections.

The first step, using MD simulations, is to analyze the variation of the barrier height due to thermal motion of the solid. This analysis determines the heavy oscillator parameters, as is shown in Sec. V A. Once the oscillator parameters are determined, an assessment of the model is made in Sec. V B. For further comparison, the same data are used to construct a bath of phonon modes for which the dynamics is solved by the surrogate Hamiltonian method.[61]

A. MD simulations for characterizing barrier motion

Concentrating on crystal-hydrogen coupling in the barrier region, a Hamiltonian, replacing that of Eq. (4.1) is constructed:

$$\hat{\mathbf{H}}=H_s(\hat{\mathbf{P}}_z,\hat{\mathbf{Z}})+\frac{\hat{\mathbf{P}}^2}{2M}+\frac{1}{2}M\omega^2\hat{\mathbf{R}}^2+V(\hat{\mathbf{Z}},\hat{\mathbf{R}}). \tag{5.1}$$

This model is aimed at studying the effects of crystal motion, so the nonadiabatic effects are neglected. The lattice motion is represented by a single harmonic oscillator with coordinate R, mass M, and frequency ω. The hydrogen motion is restricted to one dimension along the tunneling path Z. The effect of the two additional degrees of freedom was taken approximately into account by the VAA.[8,71–75] In this model, the coupling of the hydrogen and the lattice reduces to

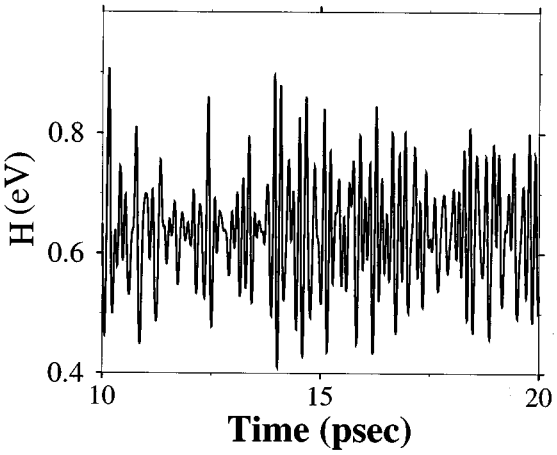

FIG. 8. Clocking the barrier motion. The barrier height h_b shown in Fig. 3 is recorded as a function of time, during a molecular-dynamics (MD) simulation of the lattice motion. A segment of 10 ps is shown.

$$V(\hat{\mathbf{Z}},\hat{\mathbf{R}})=f(Z)(bR+Ae^{-\gamma|R-R_1|}), \tag{5.2}$$

where bR represents the basic coupling, linear in the heavy oscillator coordinate, with force constant b. The function $f(Z)$ localizes the coupling to the barrier region at Z_o. The extent of localization is determined by the parameter σ,

$$f(Z)=e^{-(Z-Z_o)^2/2\sigma^2}. \tag{5.3}$$

The exponential term in Eq. (5.2) represents the H-Ni repulsion at large extensions. For every crystal configuration R, the potential $V(\hat{\mathbf{Z}},\hat{\mathbf{R}})$ represents the correction to the hydrogen adiabatic potential $V_s(Z)$. It is convenient to define the barrier height $h_b(R)$ as the difference between the potential at the top of the barrier and that at the bottom of the subsurface well. Near $R=0$ the barrier height h_b is a monotonic ascending function of R. As the oscillator moves to the negative-R direction, the barrier for tunneling is lowered, while it is elevated as the heavy oscillator displacement is extended to the positive-R directions.

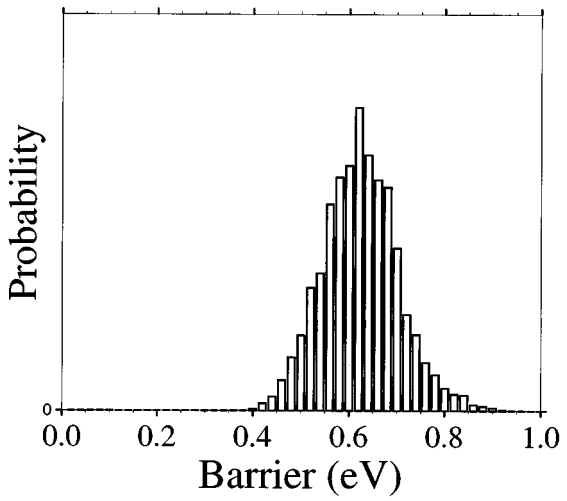

FIG. 9. The distribution function of barrier heights h_b obtained from the MD simulation. The average barrier was found to be 0.62 eV. The distribution width for the simulation temperature (90 K) is $\sigma=0.079$ eV.

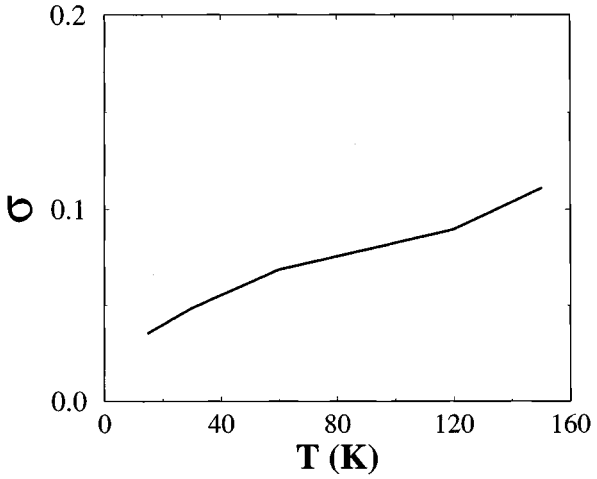

FIG. 10. The variance in the barrier distribution in eV as a function of temperature.

To characterize the coupling features (namely, the parameters b and σ), MD simulations are used. The change in the adiabatic potential V is reduced to a single parameter—it is characterized by the change in the barrier height h_b. This quantity is calculated for different configurations of the solid atoms as dictated by their thermal motion. The calculations also account for the presence of subsurface hydrogen in the metastable well. The MD simulations were initiated with a thermalization phase which lasted 10 ps. During the simulation, the mass of the hydrogen atom was artificially increased to 5000 amu in order to prevent its migration to other sites. After the thermalization stage the system evolution was followed for an additional 10 ps. At each time step of the simulation during this second stage, the barrier height h_b was registered. The estimation of h_b was performed by determining the potential energy for a set of hydrogen atom positions along a line that passes from the subsurface site to the threefold hollow surface site along the Z coordinate.

The values of h_b result from thermal fluctuations at a specific hydrogenic site in the nickel crystal. A similar procedure employing a MD simulation was used to record the barrier height of two hydrogen atoms, where one atom is in a neighboring surface site. At the lowest barrier height, the potential of the metastable well was examined along the reaction path. Comparison to the equilibrium potential curve is shown in Fig. 3. Typical variations of h_b due to the thermal motion of the metal atoms, at 90 K, are shown in Fig. 8.

These results correspond to h_b variations during the second stage of the simulation (as noted above, the initial 10 ps served as a thermalization period for the system). Inspection of these results shows a rapid variation in the value of h_b with an occasionally dramatic change in magnitude. The distribution of the the h_b values is shown in Fig. 9.

Examining Fig. 9, a near-Gaussian distribution emerges, with an average h_b of 0.624 eV and a variance σ of 0.079 V. Similar calculations were performed for a wide range of temperatures. For all temperature values examined the barrier height distribution, was Gaussian-like. The variation of σ, as a function of surface temperature, is shown in Fig. 10. The

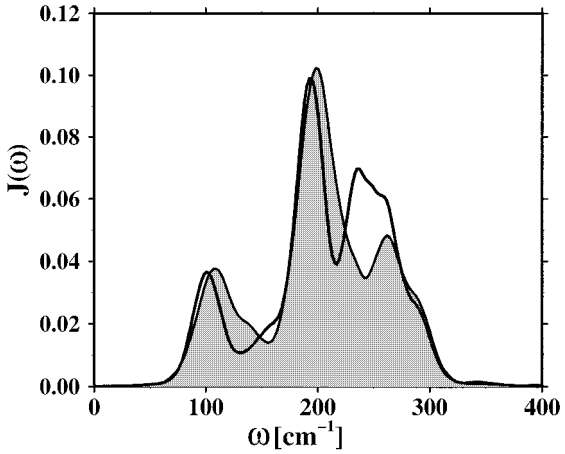

FIG. 11. The spectral density of the barrier height, determined from a MD calculation, for a single H atom in a hcp subsurface site (gray filling). The other line corresponds to the spectral density of the barrier h_b when another hydrogen atom resides on the surface in a nearby threefold fcc site.

functional dependence of σ on the temperature nearly linear increases fivefold in the range of $20\text{K} < T_s < 160$ K.

These results indicate that the magnitude of h_b changes appreciably due to the thermal fluctuations of the surface atoms. The principal frequencies are determined by calculating the spectral density of $h_b(t)$ (see Appendix C), shown in Fig. 11.

Analyzing the figure, the frequencies of the barrier fluctuations span the range of 60–300 cm^{-1}, with the dominant modes at 200 cm^{-1}. These frequencies are small in comparison to the H-atom perpendicular vibration in the subsurface well of 970 cm^{-1}. One expects that this rather large frequency ratio is sufficient to allow the neglect of correlations between the two modes. As shown below, this is not the case when tunneling motion is involved.

The presence of the surface hydrogen only slightly narrows the spectral density of the barrier height. The influence of a surface hydrogen occupying a neighboring threefold hollow site on the spectral density is negligible.

B. Lattice represented by a single-mode oscillator: Assessment

The oscillator representing the lattice dynamics can either be coupled locally to the most sensitive region of the potential or spread out. It is essential therefore to examine two rather extreme regimes. In the local coupling regime the crystal motion only influences the barrier itself, and is characterized by a small-σ parameter. The extended coupling regime is characterized by larger σ, and allows an outspread effect of the crystal motion on both the barrier and the metastable well. The two-dimensional potential surfaces corresponding to these coupling regimes are shown in Figs. 12 and 13.

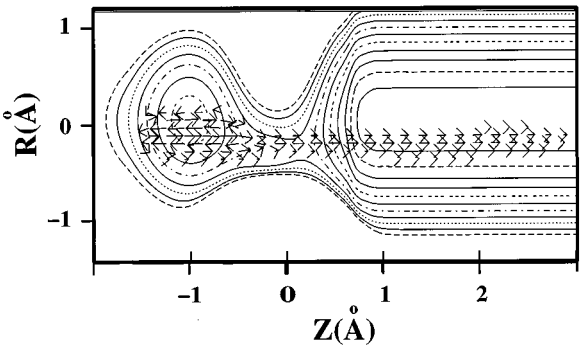

FIG. 12. Flux of a 0.35-eV tunneling state, superimposed on the potential-energy surface of the local heavy oscillator model. The potential difference between adjacent contour lines is 0.14 eV.

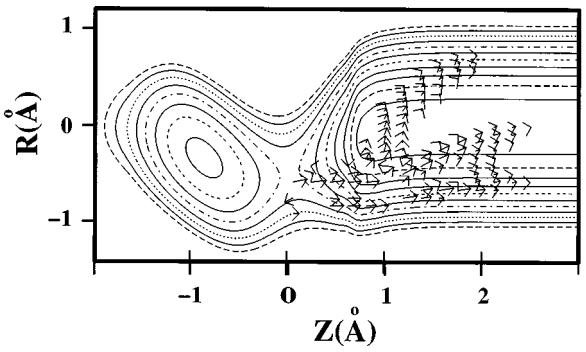

FIG. 13. Flux of a 0.26-eV tunneling state, superimposed on the potential-energy surface of the extended coupling regime. The potential difference between adjacent contour lines is 0.14 eV.

The extended coupling regime has a closer similarity to the MD simulations. This can be seen in Fig. 3, where the lowering of the barrier height is accompanied by the lowering of the metastable well potential. The parameters used for the two coupling regimes are given in Table I. The mass was chosen to represent a single nickel atom. The frequency of the oscillator was taken to be close to the maximal spectral density frequency (see Fig. 11). The strength of the coupling, the parameter b, was adjusted to the variance found for the barrier height fluctuations (Fig. 10), assuming that the heavy oscillator is in thermal equilibrium. The potential energy contour map of the two coupling regimes is shown in Figs. 12 and 13. The tunneling rates corresponding to the fully correlated 2D model of Eq. (5.2) were calculated using the method described in Ref. 8.

It is now appropriate to use this model for examining the validity of neglecting correlations between the two modes of very different frequency—the hydrogen motion and the lattice vibration. For this purpose, the tunneling rate is calculated in an uncorrelated model called the static barrier approximation. This model averages 1D tunneling rates $J_\nu(R)$ with respect to the static heavy-oscillator displacements R,

TABLE I. Parameters of the single heavy oscillator models [see Eqs. (5.1), (5.2), and (5.3) for definition of symbols].

Parameter	Local coupling	Extended coupling
M	110 000	110 000
ω (cm^{-1})	190	190
Z_o (bohr)	−0.25	−0.5
σ (bohr)	0.5	1.1
A (eV)	0.136	0.0
γ (bohr^{-1})	8.0	0.0
B (Ht bohr^{-1})	0.049	0.049

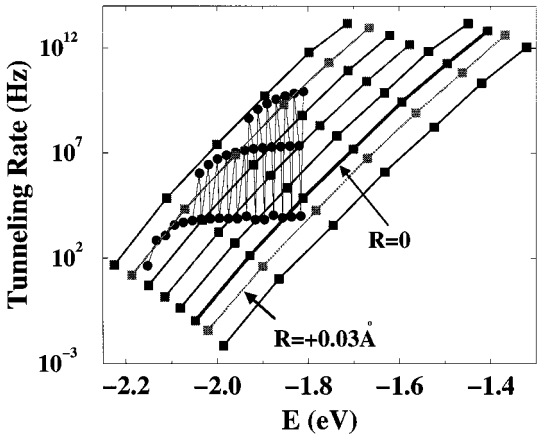

FIG. 14. Hydrogen tunneling spectra in the static barrier approximation for a variety of barrier heights (black squares). Superimposed is the 2D spectra for hydrogen tunneling coupled to a heavy oscillator (black dots). The coupling in this calculation is the extended coupling, shown in Fig. 13.

$$J(T)=\int dRP(R,T)\sum_{\nu} J_{\nu}(R)e^{-\beta E_{\nu}}, \tag{5.4}$$

where the probability density of the heavy harmonic-oscillator displacement at temperature T is $P(R,T)=\exp(-R^2/2\sigma^2)/\sqrt{2\pi\sigma}$ and $\sigma^2=\hbar\coth(\hbar\omega/2k_BT)/M\omega$. In Appendix B the static barrier approximation is studied, and Eq. (5.4) is systematically derived. Its derivation is based on two assumptions: the adiabatic approximation, where the kinetic couplings (the derivatives of the hydrogen eigenstates relative to the slow degree of freedom) are neglected, and an additional assumption that the hydrogen vibrational energies are independent of the heavy oscillator displacement. This last assumption seems plausible, at least for the local coupling regime, where the coupling only slightly modifies the metastable well shape (see Fig. 12).

Using the potential energy of Eq. (5.2) with the parameters in Table I, the tunneling rates for various metastable vibrational states were calculated. The results are shown in Figs. 14 and 15, where the fully correlated 2D tunneling rates are superimposed on 1D static-barrier rates, for various heavy-oscillator displacements. The tunneling rate of hydrogen in the extended coupling regime is shown in Fig. 14. The 2D tunneling states fall into lifetime bands. It is also seen that the energy of the 1D states is dependent on the oscillator displacement (R), signaling poor performance of the static barrier approximation. This is mainly due to the extended character of the coupling. A similar figure is shown for deuterium in a local coupling regime. Here, due to the local coupling, the energy of the tunneling states is almost independent of the deuterium location.

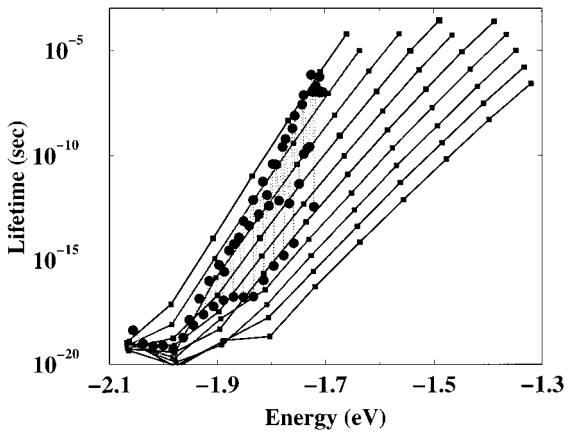

FIG. 15. The same as Fig. 14, but for deuterium, and for local coupling as shown in Fig. 12.

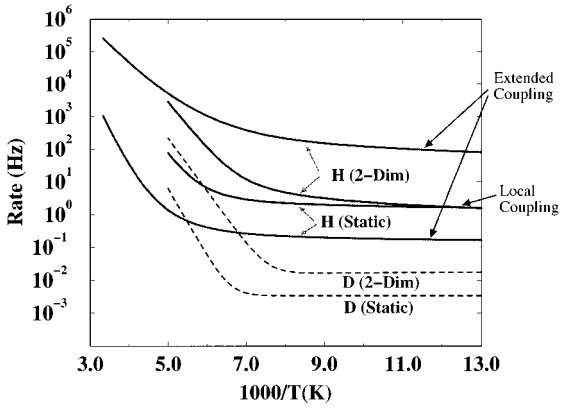

FIG. 16. Comparison of thermally averaged tunneling rates for resurfacing of hydrogen from an octahedral subsurface site. Calculations based on the local and extended coupling regimes are shown, comparing the two-dimensional model calculations with the static barrier approximation. Also shown are the local coupling regime calculations for deuterium.

It is observed in both figures that the fully correlated 2D model yields tunneling rates corresponding to large negative oscillator displacements. This hints that the uncorrelated static barrier approximation is inaccurate. Further evidence of the inadequacy of the static barrier approximation is revealed in the flux map of the full (exact) tunneling state. Examples are shown in Figs. 12 and 13. It can be seen that the tunneling flux is located mainly in the low barrier saddle point, even though this means very large and rare stretches of the heavy oscillator. Moreover, the tunneling flux represents a correlated motion of the hydrogen and the heavy oscillator.

Thermally averaged rates for the two coupling regimes are compared in Fig. 16. The isotope effect is also considered. It is clearly seen that the static approximation grossly underestimates the tunneling rate by orders of magnitude. The only combination where the static approximation is applicable is for low energy, local coupling, and light mass. In any other combination, the static calculations are very inaccurate for the estimation of tunneling rates. For deuterium this approximation is even poorer due to the smaller mass mismatch. It is also seen that, for higher temperatures, the two methods predict a different temperature dependence, namely, distinct activation energies.

An important, experimentally measurable quantity is the crossover temperature. It marks the onset of temperature independent resurfacing rates. The correlated 2D models typically have lower crossover temperatures than the static barrier models. Also, deuterium coupled to the heavy oscillator has lower crossover temperatures than hydrogen. In a previous publication,[8] a crossover temperature of 210 K was reported for the 1D/VAA approximation of hydrogen. Here, as

TABLE II. Parameters of the Gaussian decomposition of $J(\epsilon)$.

Parameter	$n=1$	$n=2$	$n=3$
A_n (eV)	1.0	2.8	1.3
ϵ_n (cm^{-1})	110	200	260
σ_n (cm^{-1})	22	15	22

can be seen in Fig. 16, the coupling to a heavy oscillator yields a markedly lower crossover temperature of 140 K for hydrogen (local coupling) and 155 K (extended coupling) compared to 130 K for deuterium. This narrowing of the T-independent range of the tunneling rates is in good qualitative agreement with experimental and other theoretical observations of quantum effects related to surface diffusion.[4–6,40,41,7]

The overall effect of the barrier motion in this model is to enhance the tunneling rate with respect to the frozen lattice calculation by one and three orders of magnitude for the local and the extended coupling regimes, respectively. This effect is known as phonon-assisted tunneling.[29] The conclusion of this section is that neglecting the correlations of different degrees of freedom, even when they seem to have different time scales, is usually inappropriate for studying tunneling dynamics.

C. Single oscillator vs bath of oscillators

In studying the influence of the bath, the next question is whether a single oscillator coupled to the barrier is an adequate model even when fully correlated. In order to study this, the tunneling rates of the single-oscillator model are compared to rates calculated by a more elaborate model: a multiphonon bath spanning the spectral density of barrier motion. In Sec. VI an even more elaborate system bath coupling will be studied.

Treating the hydrogen dynamics under the influence of a multiphonon bath is done by the use of the surrogate Hamiltonian method. This method replaces the highly structured phononic bath by a simpler bath while conserving the spectral density. A detailed description of this method is found in Ref. 61, and a short summary is given in Appendix A. The spectral density is estimated by analyzing the MD correlation functions as described in Appendix C. The estimated spectral density is shown in Fig. 11. It is convenient to employ an analytical approximation of the spectral density $J(\epsilon)$. This is done by decomposing the full spectral density function to a sum of three Gaussians:

$$J(\epsilon)\approx\sum_{n=1}^{3} A_n e^{-(\epsilon-\epsilon_n)^2/2\sigma_n^2}. \tag{5.5}$$

The parameters used here are given in Table II. The frequency range represented was set at $\omega_0=60$ cm^{-1} to $\omega_f=300$ cm^{-1}.

The coupling function $f(Z)$ [see Eq. (A4)] was chosen with parameters of the extended coupling regime as shown in Table I, and the tunneling states were calculated using the surrogate Hamiltonian method.[61] It was found that the resulting thermal tunneling rate is satisfactorily converged with the use of a bath consisting of five two-level-system modes.

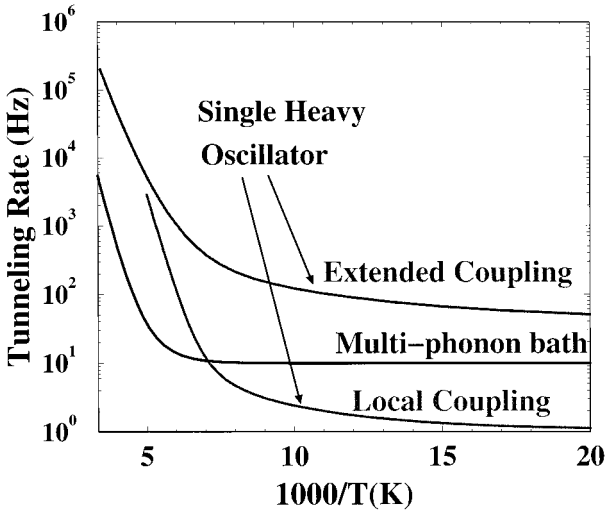

FIG. 17. Comparison of the thermal tunneling rate of resurfacing hydrogen for three models: the single-oscillator local regime, extended coupling regime, and multiphonon bath regime.

The thermal rates are shown in Fig. 17, and are compared to the 2D single heavy-oscillator rates for the local and extended models.

It is clear that the thermal tunneling obtained by the multiphonon bath model has a markedly different behavior as compared to the single-oscillator one-mode model. The temperature-independent regime spans a much larger range, where the crossover temperature is approximately 200 K compared to 140–155 K for the single-oscillator models. For low-temperature tunneling, the phonon bath rate is between that of the two single-oscillator regimes. The extended coupling regime is much more efficient in enhancing the tunneling than the phonon bath, even though both have been built from the same MD data using the same extension σ. This shows that the effect of phonon-assisted tunneling is reduced when a single oscillator is replaced by a bath of phonons. Such a conclusion is also observed by looking at the Arrhenius regime, where the activation energy for a single oscillator is lower than that of the bath.

Experimentally, the resurfacing time is of the order of hours.[2] This fact is in discrepancy with the calculated time of seconds. This discrepancy cannot be overcome by the fact that the VAA was shown to overestimate the tunneling by a factor of 5.[8] It is possible that the potential used is not accurate enough due to the extreme sensitivity of tunneling. Recent variational transition state calculations with EDIM potential produce even higher rates in the range of the single-oscillator calculation.[30] The suppression of tunneling by the multimode bath compared to the single-oscillator model suggests that an additional tunneling hindrance mechanism exists in this case. This conjecture is backed up by theoretical estimations showing that the phonon vibrations can decrease tunneling rates (see Ref. 32 for a comprehensive discussion and extensive reference list). It therefore seems necessary to reexamine the coupling of the tunneling dynamics to the lattice.

VI. RESURFACING DYNAMICS III: LATTICE REPRESENTED BY SEVERAL BATHS

The tunneling dynamics requires spatially long-range coherence. This coherence can be destroyed if uncorrelated

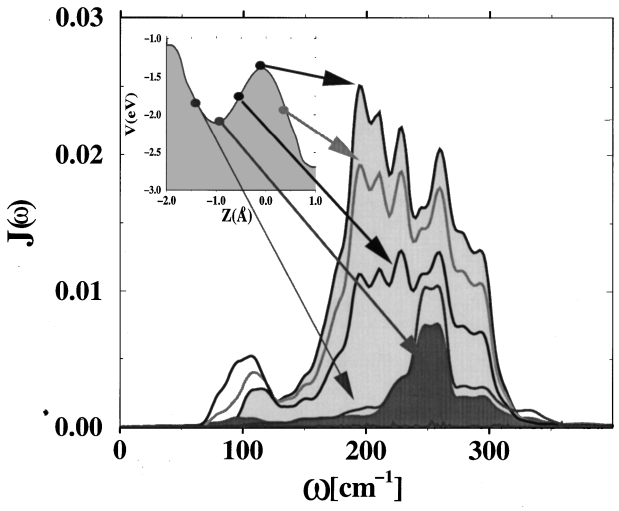

FIG. 18. Spectral densities of the system-bath interaction, taken at various locations of the hydrogen atom on the reaction path. These results are based on a molecular-dynamics simulation at 90 K.

bath dynamics influences different parts of the potential along the tunneling route. To study this possibility, a model is constructed by coupling the primary tunneling degree of freedom to several multiphonon baths. The surrogate Hamiltonian method[61] is employed, enabling a description of tunneling coupled to several dissipative baths of phonons. These baths reflect in a realistic manner the hydrogen-lattice interaction.

The Hamiltonian of Eq. (4.1) becomes the Hamiltonian of a primary system interacting with phonon baths,

$$\hat{\mathbf{H}}=\hat{\mathbf{T}}+\hat{\mathbf{V}}_s(Z)+\sum_{i,k}\epsilon_{i,k}\mathbf{b}_{i,k}^{\dagger}\mathbf{b}_{i,k}+\sum_i f_i(Z)\sum_k V_{i,k}(\mathbf{b}_{i,k}^{\dagger}+\mathbf{b}_{i,k}). \tag{6.1}$$

Here $\hat{\mathbf{T}}$ represents the kinetic-energy operator for the hydrogen-atom motion, and $\hat{\mathbf{V}}_s(Z)$ is the corresponding potential energy represented by the average reaction path. There are several phonon baths, indexed by i, each described by a sum of free-phonon-energy terms, indexed by k, where $\epsilon_{i,k}=\hbar\omega_{i,k}$ is the energy of the kth phonon mode of the ith bath (the ground-state energies of the phonons are neglected), and $\hat{\mathbf{n}}_{i,k}=\hat{\mathbf{b}}_{i,k}^{\dagger}\hat{\mathbf{b}}_{i,k}$ is the occupation number, where $\hat{\mathbf{b}}_{i,k}=\sqrt{m_{i,k}\omega_{i,k}/\hbar}\,\hat{\mathbf{x}}_{\mathbf{i,k}}+i\hat{\mathbf{p}}_{i,k}/\sqrt{m_{i,k}\hbar\omega_{i,k}}$, and $m_{i,k}$, $\hat{\mathbf{x}}_{i,k}$, and $\hat{\mathbf{p}}_{i,k}$ are, respectively, the mass, coordinate, and momentum of the (i,k)th oscillator of the bath.

The spectral density is calculated for various positions of the hydrogen atom along the reaction path potential using a MD simulation. Analysis of the MD data discussed in Appendix C results in a spectral density which is dependent on the position of the hydrogen atom, as shown in Fig. 18.

A model consisting of three independent phononbaths is sufficient to describe the spectral density

$$J(\epsilon,Z)=\sum_i |f_i(Z)|^2 J_i(\epsilon), \tag{6.2}$$

where Gaussian functions in Z are used to localize the phonon interaction:

$$f_i(Z)=e^{-(Z-Z_o i)^2/2\zeta_i^2}. \tag{6.3}$$

The local spectral densities are also cast into sums of Gaussians in ϵ localized in energy:

$$J_i(\epsilon)=\sum_k |V_{i,k}|^2\delta(\epsilon-\epsilon_{i,k})=\sum_{\alpha=1}^{2} A_{i,\alpha}e^{-(\epsilon-\epsilon_{i,\alpha})^2/2\sigma_{i,\alpha}^2}. \tag{6.4}$$

The parameters describing the spectral densities are extracted from a molecular dynamics simulation, and are summarized in Table III.

The first bath ($i=1$) is localized on the barrier peak position like the bath of Sec. V C, and has a wide frequency range. The second bath ($i=2$) is localized in the metastable well minimum, with frequencies centered around 250 cm^{-1}. The third bath with low frequency is localized on the repulsive slope.

The calculation was performed using three bath modes for each of the three baths. Calculations with a larger number of modes have confirmed reasonable convergence. The calculated thermal tunneling rates are shown in Fig. 19, and compared with the frozen lattice rates and with the single bath rates of Sec. V C.

The striking feature is that the composite bath, consisting of three different phonon baths, imposes a drastic reduction of the tunneling rate compared to the enhancement caused by the single-phonon bath with coupling localized on the barrier. The rate is decreased by two orders of magnitude, and it plunges below the frozen lattice rate.

Thus the overall effect of the phonons is to hinder hydrogen tunneling. This observation is in contrast to surface diffusion and resurfacing calculations of Truhlar and co-workers,[29,30] for which a mechanism of phonon-assisted tunneling is reported (see Ref. 61 for a discussion of surface diffusion on nickel). The three-phonon-bath model resurfacing rates are still higher than experimental resurfacing rates by two orders of magnitude.

TABLE III. Parameters of the spectral densities.

i	Z_i (bohr)	ζ_i (bohr)	$A_{i,1}$ (Ht)	$\epsilon_{i,1}$ (cm^{-1})	$\sigma_{i,1}$ (cm^{-1})	$A_{i,2}$ (Ht)	$\epsilon_{i,2}$ (cm^{-1})	$\sigma_{i,2}$ (cm^{-1})
1	0	0.8	0.025	197.5	21.9	0.021	254.6	26.3
2	−2.5	1.56	0.01	254	26.3	0		
3	+0.945	0.325	0.0125	94.3	16.7	0		

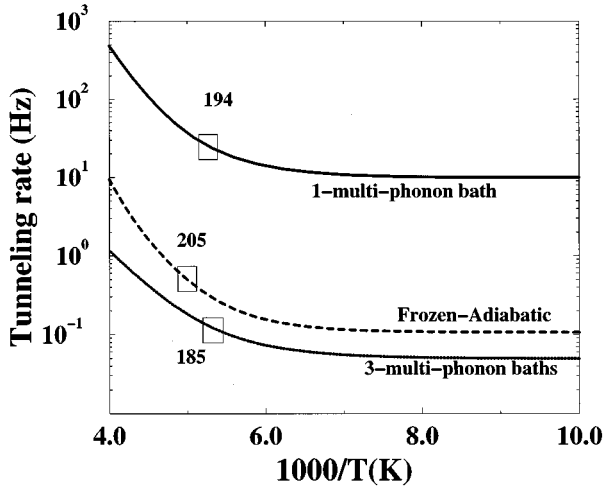

FIG. 19. The tunneling rate for three adiabatic approximations: a frozen lattice, a phonon bath consisting of a phonon bath coupled to the barrier, and three phonon baths coupled to the full extent of the reaction coordinate.

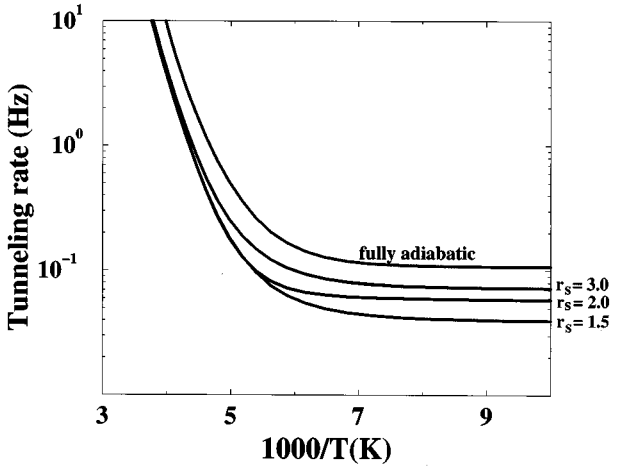

FIG. 20. The thermal tunneling rate of resurfacing hydrogen, shown for three metallic electron densities and for the adiabatic tunneling.

Based on these results, two fundamental types of bath influence on tunneling can be recognized. They can generally be distinguished by the symmetry of the coupling function $f(Z)$ with respect to the location of the barrier peak (taken at $Z=0$). If $f(Z)$ is an even function of Z, the phonon vibrations cause the potential on both sides of the barrier to oscillate in-phase. In this case the delicate long-range coherence of the hydrogenic wave function is not disturbed, and the tunneling is assisted by the occasional lowering of the barrier height. On the other hand, if $f(Z)$ is an odd function of Z, the potential surface on the phonon motion causes the two sides of the barrier to oscillate out of phase, and this destroys the long-range coherence of the hydronic wave function. This results in a severe hindrance of the tunneling rate.

VII. RESURFACING DYNAMICS IV: NONADIABATIC EFFECTS

The exponential sensitivity of the tunneling process to almost any dynamical factor requires a serious consideration of nonadiabatic effects caused by the interaction between the hydrogen atom and the conduction electrons of metals.[76,77] The nonadiabatic effect depends on the coupling parameters of the specific system. The present system can be characterized by a composite Ohmic bath in which the spectral density is linear in the excitation energy.

The dynamics of coupling the primary system to nonadiabatic interaction has been developed using the surrogate Hamiltonian method.[61] Here the general scheme is applied to the resurfacing phenomena. The thermal tunneling rate was calculated as a function of the electron density, and is shown in Fig. 20. It can be seen that the nonadiabatic interactions have, in general, a damping effect on the tunneling rate, which increases with the metal electron density. The upper bound of the damping effect is approximately a factor of 3 for the temperature range shown. The crossover temperature is reduced slightly by about 5 K at the higher electron densities considered. From the EAM calculation the electron density is directly obtained, yielding a density parameter of $r_s=2.1$ for the subsurface hcp site. It is, however, not clear what is the exact value of the electron density which needs to be used in the model, since part of the interaction between hydrogen and the electron-excitations is accounted for just by using the adiabatic potential. Thus the calculation was performed for several values of the electron density, enabling a parametric study. The results are shown in Fig. 20. Based on these calculations, it is concluded that, for this process, the nonadiabatic interactions reduce the resurfacing rates of hydrogen, by a factor of approximately 2–3.

VIII. DESORPTION OF HYDROGEN FROM NICKEL (111)

The final step of the hydrogen odyssey in nickel is the recombinative desorption. The reaction rates are determined by calculating the width of the recombination resonances. The potential surface shown in Fig. 4 was used. The general strategy is to view the reaction as a unimolecular dissociation

$$\mathbf{H_2M}\rightarrow\mathbf{H_2}+\mathbf{M}. \tag{8.1}$$

The method of calculation is similar to the technique of estimating tunneling rates described in Ref. 8. The first step is to calculate the eigenstates of the desorption well by blocking the exit channels to both the molecular species and surface diffusion. In this fashion, 48 vibrational eigenfunctions of the well were calculated, up to and over the desorption barrier height. Next, the exit channel to the molecular species was unblocked and a negative imaginary potential was placed at the far molecular asymptote. Desorption eigenstates were then calculated by filtering the states with outgoing only boundary conditions using the Greenian filtering operator, in an identical manner to the calculation of tunneling eigenstates shown in Ref. 8. The first ten states were below the threshold for reaction. The eigenvalues of the consecutive 38 states are shown in Fig. 21. It is seen that two kinds of desorption mechanisms exist. One is due to tunneling through the small adsorption barrier, while the other corresponds to over-the-barrier Feschbach resonances. The microscopic rates were thermally averaged and the resulting thermal desorption rates are shown in Fig. 22.

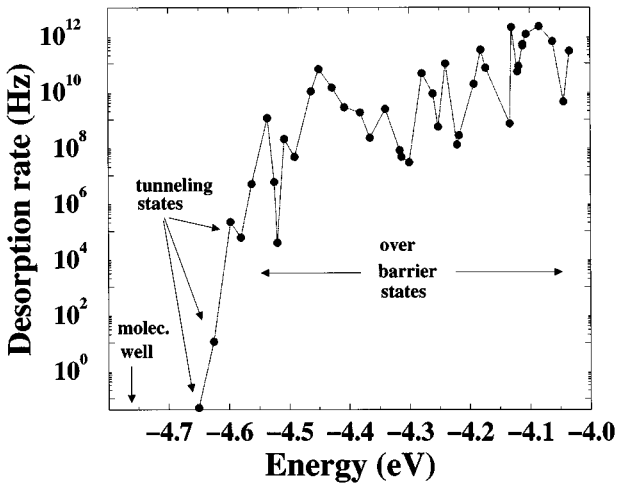

FIG. 21. The desorption spectrum of surface hydrogen based on the PES of Fig. 4. The potential-energy minimum of molecular H_2 is marked. The first three states of lowest energy are tunneling states through the 0.17-eV adsorption barrier. The other states are over-the-barrier resonances. Lines connecting the resonance points are a guide for the eye.

The thermal rate for the relevant temperature range can be fit by using a double Arrhenius curve, as discussed in Sec. IX C. This limited dimensional approximation results in a crude upper estimate of the recombination rate. The influence of lattice dynamics was not analyzed for this reaction.

IX. KINETIC MODEL FOR THE TPD SIGNAL

In order to compare the calculated recombination TPD rates to experimental data, the individual rates have to be combined into a kinetic model. The main assumptions of the model are summarized as follows:

(1) Hydrogen readily adsorbs on the nickel surface. Molecular hydrogen dissociates, and the hydrogen fragment can occupy four types of surface sites, two of which are metastable (on-top and bridge). The stable sites are the two threefold sites.

(2) Atomic hydrogen, coming from the gas phase, readily enters the bulk and thermalizes in interstitial sites. The most stable bulk sites are those directly underneath the threefold hollow surface sites.

(3) The recombination of two surface hydrogen atoms is endothermic, by about ~ 0.5 eV, and the desorption process is activated by a barrier of ~ 0.67 eV.

(4) A hydrogen atom in the subsurface site can resurface by tunneling through a 0.6-eV barrier to a vacant threefold hollow site. The thermal rate of this process has been examined using different models and levels of approximation.

(5) When a hydrogen atom occupies a surface threefold hollow site, it blocks the exit of a subsurface hydrogen atom (see Fig. 5), raising the resurfacing barrier to 1.2 eV. Two conclusions follow from this observation:

(i) A high occupation number of hcp sites causes a decrease in the resurfacing rate. This is called *the capping effect*.

(ii) A direct reaction mechanism, between a subsurface hydrogen atom and a surface on-top hydrogen, cannot explain the low-temperature bulk-surface recombination. This conclusion is strengthened by recent experimental measurements, which show that bulk-surface recombination products have a wide angular distribution.[78]

(6) The subsurface hcp site is metastable with respect to a surface site. The energy difference is about 0.4 eV in potential energy and 0.23 eV in zero-point vibrational energy, totaling to 0.63 eV. It follows that, immediately after resurfacing, the hydrogen is very *hot*, and interacts rapidly with a surface hydrogen located in a neighboring site.

(7) The relaxation rate of a *hot* hydrogen atom is primarily due to nonadiabatic electron-hole pair excitations.[61]

These points are used to construct a kinetic model for the bulk-surface recombination process. In this model the subsurface-surface reaction is broken into two kinetically distinct stages. First, a resurfacing stage, where excited hydrogen is formed after tunneling out of the subsurface. Next the *hot* hydrogen finds a thermalized surface hydrogen and reacts with it. The possibility of reaction among two *hot* hydrogens is negligible, since the hot hydrogens relax extremely fast relative to their formation rate. A further simplification in the model is that the difference between fcc and hcp sites is neglected due to their fast equilibration via surface diffusion.[61,7,41] The kinetic equations describing the combined process become:

$$\frac{d[\mathbf{B}]}{dt} = -K_b[\mathbf{B}](1-[\mathbf{S}]-[\mathbf{S}^*]),$$

$$\frac{d[\mathbf{S}^*]}{dt} = +K_b[\mathbf{B}](1-[\mathbf{S}]-[\mathbf{S}^*]) - \gamma[\mathbf{S}^*] - k^*[\mathbf{S}^*][\mathbf{S}], \tag{9.1}$$

$$\frac{d[\mathbf{S}]}{dt} = \gamma[\mathbf{S}^*] - k^*[\mathbf{S}^*][\mathbf{S}] - 2k[\mathbf{S}]^2,$$

$$T = T_o + \alpha t,$$

where all occupation numbers are *per surface site*, and $[B]$ is the occupation number of subsurface hydrogen, $[S]$ is the occupation number of thermalized surface hydrogen atoms (H), $[S^*]$ is the occupation number of hot resurfacing hydro-

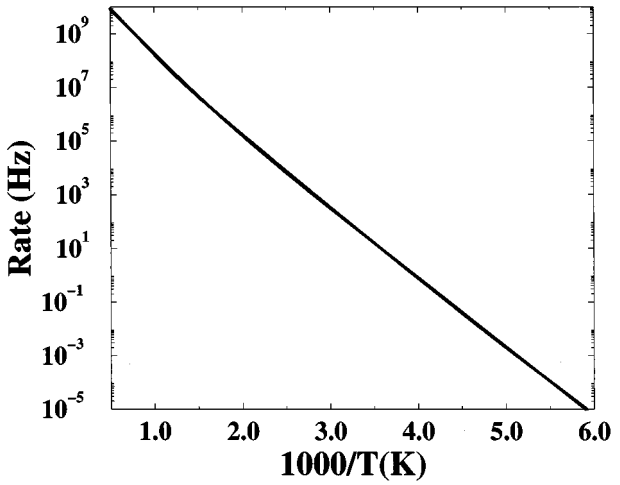

FIG. 22. The thermal recombination rate of surface hydrogen. Also shown is the double Arrhenius curve used to fit the data.

TABLE IV. The different estimations of the hydrogen-resurfacing rates crossover temperatures and activation energies.

	Adiabatic potential	Number of H DOF's	Lattice motion	Electronic nonadiabaticity	Rate (Hz) [a]	T_c (K)	E_a (eV)
1	EDIM	1	frozen	neglect	10^{+3}	200	0.47
2	EDIM+VAA	1D	frozen	neglect	0.5	200	0.57
3	EDIM	3D	frozen	neglect	0.1	205	0.5
4	EDIM+VAA	1D	1-mode/Local Coup./Stat. Bar.	neglect	0.3	200	0.27
5	EDIM+VAA	1D	1-mode/Local Coup.	neglect	1	140	0.26
6	EDIM+VAA	1D	1-mode/Extended Coup.	neglect	$7\times10^{+1}$	156	0.21
7	EDIM+VAA	1D	1-multiphonon Ext. Coup.	neglect	10^{+1}	194	0.26
8	EDIM+VAA	1D	3-multiphonon-baths	neglect	5×10^{-2}	185	0.15
9	EDIM+VAA	1D	frozen	e-hole bath	2×10^{-2}	190	0.32
10	Ref. 30	TST [b]	partition function	neglect	10^{+4}	130	0.33

[a]Rate at zero temperature.
[b]TST-tunneling-corrected variational transition state theory.

gen atoms (H*), K_b is the thermal resurfacing rate constant, γ is the relaxation rate constant of excited hydrogen, k^* is the thermal rate constant of the reaction $H^*+H\rightarrow H_2$, and k is the thermal rate constant of the reaction $H+H\rightarrow H_2$, and α is the surface heating rate, taken as 2 K s^{-1} in accord with the experimental value.

The TPD signal is given by the desorption rate

$$\frac{d[\mathbf{G}]}{dt}=k^*[\mathbf{S}^*][\mathbf{S}]+k[\mathbf{S}]^2, \tag{9.2}$$

where $[\mathbf{G}]$ is the number of desorbed H_2 molecules per surface site. In the following sections the rate constants are estimated, based on the different calculations described in the present study.

A. Resurfacing rate K_b

Estimating the tunneling rates is a difficult task due to the exponential sensitivity and the strong dependence on the dimensionality of the process. Table IV summarizes the hierarchy of approximation used for the hydrogen tunneling resurfacing rates. For completion the TST calculation of Ref. 30 is included in the table, which is two orders of magnitude faster than the frozen lattice calculation at 0 K. The tunneling rates as a function of temperature for the different approximations are summarized in Fig. 23.

It is clear from this figure that the different models predict rates differing by five orders of magnitude for the same process. The tunneling rate constants were fit to a universal form

$$K(T)=K_o\exp\left(-\frac{E_a}{k_BT_a}\left[\frac{\frac{T_a}{6T}-1}{\left[1+\left(\frac{T_a}{T}\right)^n\right]\left(1+\frac{T_a}{T}\right)}\right]\right). \tag{9.3}$$

This expression contains four parameters: (i) $T_a=1.2T_c$, where T_c is the crossover temperature; (ii) E_a is the activation energy of the Arrhenius part of the rate constant temperature dependence; (iii) K_o is the temperature independent rate; and (iv) n is a parameter, describing the curvature of the crossover region. The most elaborate phonon model, using three baths (Sec. VI), estimates the temperature-independent tunneling rate as $K_o=0.05$ s^{-1}, the crossover temperature as $T_c=185$ K and $E_a=0.87$ eV. However, the nonadiabatic interactions shown in Fig. 23 exhibit an additional decrease in K_o by a factor of 2 and of T_c by 5 K. In Ref. 8 it was shown that the reduced dimensional VAA causes an overestimation of K_o by a factor of 5, and of the crossover temperature T_c by 10 K. Based on these considerations the following parameters were chosen for the universal function representing K_b: $T_c=170$ K, $K_o=0.005$ s^{-1}, $E_a=0.87$ eV, and $n=5.1$.

B. Relaxation rate γ

The resurfacing hydrogen atom has an excess energy of 0.63 eV with respect to a surface hydrogen at its ground state. This is due to the 0.4-eV difference in the binding energies of surface and subsurface hydrogen atoms with an additional 0.23 eV, the difference in zero-point energy, and the surface hydrogen. This excess energy allows the *hot* hydrogen to wander freely on the surface. The relaxation mechanism causes loss of the hot hydrogen energy due to

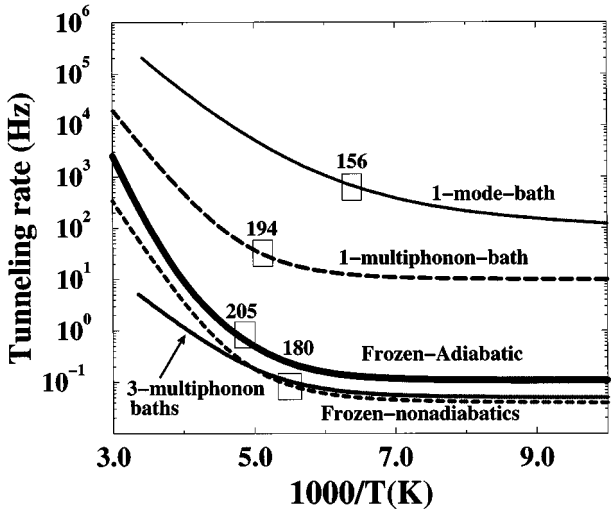

FIG. 23. The thermal tunneling rate of resurfacing hydrogen, shown for the various model calculations. The boxes indicate the crossover temperature.

electron-hole pair excitations. The vibrational line broadening of the transverse mode was calculated in Ref. 61, and it was found to be 23 cm^{-1}, yielding the relaxation rate $\gamma = 2\times10^{12}$–$4\times10^{12}\ s^{-1}$. A similar value is obtained for the translational energy relaxation due to the nonadiabatic friction.[61] Hence a value of $\gamma = 2\times10^{12}\ s^{-1}$ is assumed in the present kinetic model.

C. Recombination rate *k*

The surface reaction of the hydrogen recombination was discussed in Sec. VIII. The rate constant is well fit by a double Arrhenius function

$$k(T) = A_1 e^{-E_1/k_B T} + A_2 e^{-E_2/k_B T}, \tag{9.4}$$

where the following parameters are used: $E_1 = 0.6$ eV, $E_2 = 0.8$ eV, $A_1 = 1.5\times10^{10}\ s^{-1}$, and $A_2 = 4.1\times10^{11}\ s^{-1}$.

D. ''Hot'' hydrogen recombination rate k^*

The recombination reaction is activated, and therefore enhanced by the excitation of one of the participating hydrogen atoms. For this reason the excess energy of the resurfacing hydrogen can promote the reaction. This enhancement is estimated by lowering the activation energies E_1 and E_2 in the thermal-reaction-rate expression Eq. (9.4) by E_{xc}. Next, the kinetic prefactor is enlarged. This is due to the fact that the correlated motion of the bulk and surface atoms can have a strong effect. The analysis in this study has shown that such correlated effects, for low probability processes can enhance the rates by orders of magnitude. An example for this is seen in Sec. V B, where correlation effects enhance the tunneling rates by three orders of magnitude. Since a detailed calculation is prohibitively expensive at this stage, the prefactors are taken as parameters, their value increased by factors of 10 and 100 compared to the thermalized reaction prefactors. Summing up, the rate constant is given by Eq. (9.4) with the following parameters: $E_1 = 0.026$ eV and $E_2 = 0.17$ eV, $A_1 = 1.5\times10^{11}$ and $1.5\times10^{12}\ s^{-1}$, and $A_2 = 4.1\times10^{12}$ and $4.1\times10^{13}\ s^{-1}$.

E. TPD signal

Analysis of the kinetic model of Eqs. (9.1) shows that the number of excited hydrogen atoms on the surface, $[\mathbf{S}]^*$, is created by a relatively slow process, and destroyed by a fast process. This prohibits any attempt to solve Eqs. (9.1) directly. However, S^* is at all times extremely small, and thus changes slowly. Setting $d[\mathbf{S}^*]/dt = 0$ in Eq. (9.1) yields the set of equations:

$$\frac{d[\mathbf{B}]}{dt} = -K_b[\mathbf{B}](1-[\mathbf{S}]-[\mathbf{S}^*]),$$

$$\frac{d[\mathbf{S}]}{dt} = \gamma[\mathbf{S}^*] - k^*[\mathbf{S}^*][\mathbf{S}] - 2k[\mathbf{S}]^2, \tag{9.5}$$

$$[\mathbf{S}^*] = \frac{K_b[\mathbf{B}](1-[\mathbf{S}])}{K_b[\mathbf{B}]+\gamma+k^*[\mathbf{S}]},$$

$$T = T_o + \alpha t.$$

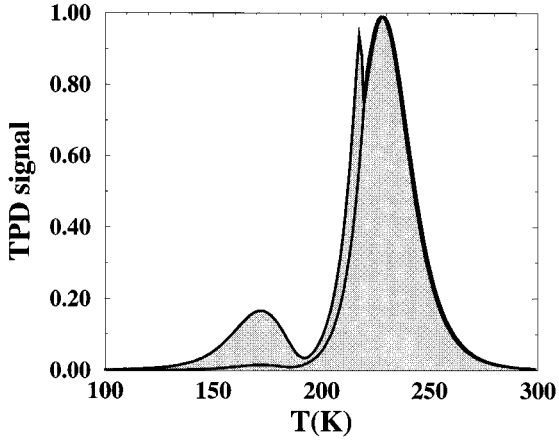

FIG. 24. The calculated TPD spectra for bulk hydrogen desorption under the proposed kinetic model. The filled line corresponds to the case where the prefactors of the excited reaction rate constants are increased by a factor of 100 relative to those of the thermal reaction. The solid line corresponds to an increase of a factor of 10.

This set of coupled equations is numerically integrated. The stability and accuracy has been checked by monitoring the identity $2[\mathbf{G}]+[\mathbf{B}]+[\mathbf{S}]=[\mathbf{B}]_o$ where $[\mathbf{B}]_o$ is the initial bulk content of hydrogen. It is assumed that the surface is initially clean.

The TPD simulated results with the initial bulk content $B_o = 1.5$ and initial temperature $T_o = 80$ K are shown in Fig. 24. Two spectra for the two sets of prefactors used to estimate k^* are displayed. In both cases, two peaks are observed. However, the magnitude of the low-temperature peak, centered at 170 K, is very sensitive to the reaction-rate constant used. The relaxation rate of hot hydrogen is fast and the surface is rather quickly filled, so that at a temperature of 190 K the creation of excited hydrogen is almost halted completely. This is a result of the *capping effect*. At higher temperatures, around 200 K, the surface-surface recombination sets in, and the surface is quickly depleted. This enables formation of more hot hydrogen atoms, and the two mechanisms of desorption work simultaneously. At 210 K, the resurfacing is so fast that the bulk is emptied almost instantly, and the hot hydrogen recombination stops. This causes a drastic decrease of the TPD rate seen as the sharp peak at 215 K. This peak is not seen when the hot hydrogen reaction is slow. By the time the temperature reaches 230 K, the surface coverage is depleted enough for the recombination reaction to slow down, and the TPD signal gradually drops.

The TPD experiment also shows two peaks,[2] at approximately 200 and 350 K, respectively. The peak at 200 K is of larger amplitude than the one at 350 K. This is attributed to the complete depletion of the bulk at low temperature. During this depletion a large fraction of the hydrogen desorbs, while the rest remains thermalized on the surface. At higher temperatures, around 350 K, the remaining surface species desorb.

Qualitatively, the dynamical calculations and the kinetic model presented confirm the conjecture that the low-temperature peak observed experimentally is due to the subsurface-surface hydrogen reaction. However, quantitatively the calculated results do not fit the experimental data.

The location of the surface reaction TPD peak is at 230 K compared to a higher experimental peak at 350 K. This discrepancy is probably due to the reduced dimensionality approximations which overestimate the reaction rates. Dissipation effects, in analogy to their influence on the resurfacing process, can also hinder the recombination reaction.

As for the low-temperature peak, the location is close to that observed in the experiments (180 K); however, the experimental results indicate that most of the bulk hydrogen is depleted at this temperature, which, due to the capping effect can only be explained by a very efficient reaction between the hot hydrogen and a desorbed hydrogen. It is seen that, increasing the reaction rate by a factor of 100, allowing for correlation effects still cannot explain the efficient depletion of bulk sites. One possible source for this discrepancy is the effect of occupied neighboring subsurface sites. The hydrogen-hydrogen repulsion in the bulk can increase the hydrogen metastability in the subsurface site, making the emitted hot hydrogen atoms even hotter. This mechanism is able to explain the efficient reaction rate, and shows that the first TPD peak has the flavor of a transient macroscopic phase transition.

X. OVERVIEW

The long journey through the different possible routes of hydrogen in nickel has been aimed at unraveling the story of subsurface-surface recombination of hydrogen. The final picture is still sketchy, and most details are missing. However, the framework that has been set supports the experimental evidence for the interesting chemical mechanism involving bulk hydrogen.[2,78] The final kinetic model contains conditions for the appearance of an additional low-temperature TPD peak, attributed to the existence of subsurface hydrogen.

However, the most interesting stories of the odyssey have been collected on the way. The combined process is extremely involved. Rationalizing it requires disassembling to individual events. The unifying factor for all events was the EDIM potential used for all processes studied. This potential enabled the identification of stable metastable subsurface and surface hydrogen species. This identification allows us to break up the process into two main parts: the resurfacing of subsurface hydrogen, and recombination desorption.

The resurfacing step conceptually seems simple, a direct transport from one potential well to a lower one in the energy surface well. A detailed analysis has revealed a convoluted picture, dominated by tunneling. The extreme sensitivity of tunneling to any dynamical or environmental factors can lead investigation astray. As is evident from Table IV, nine different approximations for the resurfacing process have been analyzed. The rate calculated by each of the approximation differs from the previous one by orders of magnitude. When checked, rigorously simple models fail. One source of error is due to cutting down the dimensionality of the problem. This has been the conclusion of a previous paper,[8] which show the failure of reduced-dimensional approximations for tunneling dynamics. Even the best variationally corrected 1D method, which includes the perpendicular zero-point energy, overestimates the tunneling at low temperature by a factor of 5.

Even more involved is the influence of the lattice motion of the heavy nickel atoms on the hydrogen tunneling dynamics. The most obvious effect is the casual decrease of the barrier height by the fluctuating lattice. The investigation started on the naïve assumption that an adiabatic separation of the fast hydrogen from the heavy nickel degrees of freedom is possible. A single-mode representation model of the bath dynamics was constructed to test this hypothesis. The result was a complete failure of the adiabatic separation. The tunneling dynamics was found to be highly correlated. The lesson learned is that an approximation that is absolutely reasonable for describing majority events of the hydrogen dynamical processes, such as the vibrational motion in the potential well, is inappropriate to describe the minute events of tunneling.

The importance of the correlated tunneling motion gave rise to the suspicion that the naive description of the bath by a single mode is misleading. It was expected that the many uncorrelated bath modes could destroy the system bath correlation and interfere with the tunneling motion. In order to be able to study such a process, a dynamical description of the bath was developed: the surrogate Hamiltonian approach.

The surrogate Hamiltonian approach replaces the infinite many-body lattice dynamics by a representative finite Hamiltonian composed of two-level systems. The success of the method relies on the observation that, for finite time, a complete resolution of the energy spectrum is not required. By sampling the spectral density of the bath in an appropriate fashion, the method systematically converges. To obtain the spectral density a molecular-dynamics simulation of the lattice motion was performed based on the same EDIM potential. As expected, the multiphonon bath assists the tunneling, but with a reduced effect compared to the single mode bath.

Tunneling dynamics with a fluctuating bath coupled only to the barrier region can be classified as phonon-assisted tunneling. In contrast, shaking the potential well of subsurface hydrogen via the phonon dynamics has been shown to prohibit tunneling.[32] For hydrogen in nickel, both effects are operative. The balance between enhancement and suppression caused by phonon dynamics is delicate. Only a quantitative, elaborate approach can determine the total phononic impact on hydrogen tunneling. For the resurfacing dynamics an analysis using the the spectral density calculated along the reaction path has shown that tunneling suppression overcomes the enhancement.

Electronic nonadiabatic effects are are also able to suppress the tunneling. Electronic friction is well established for high velocities. Computations comparing tunneling rates on a single or two-crossing Born-Oppenheim potential-energy surface shows extreme tunneling suppression in the nonadiabatic case.[79] Nevertheless, calculations using the surrogate Hamiltonian method show only a small effect considering the electron density in nickel obtained from the EAM calculation.

The tunneling dynamics suggests that there should be a significant isotope effect where the lighter isotope is faster. Conflicting effects can reverse this trend. The tight bottleneck for resurfacing leads to a large adiabatic correction due to perpendicular zero-point energy which favors the heavy isotope. The coupling to the phonon bath is also influenced by the mass ratio. Since these conflicting effects are different

for different temperatures, a comparative isotopic study is useful.

Only a comprehensive study of all possible effects on the resurfacing dynamics allows a balanced estimation of the conflicting effects. Quantitatively the combined calculated resurfacing rate is too fast, predicting that even at zero temperature subsurface hydrogen will resurface on a time scale of minutes. Experimentally when the surface hydrogen is removed, a clean nickel surface is stable for hours. In order to evaluate this discrepancy, more quantitative experiments are required, in which the resurfacing rate is measured as a function of temperature for both hydrogen and deuterium.

The surface recombination reaction leading to desorption can also be studied independently. The high-temperature peak at 350 K is attributed to this reaction. This process was simulated using a quantum-mechanical two degrees of freedom model. The rate was calculated from desorption resonances. The location of the calculated recombination peak was at 230 K, deviating from the experimental 350-K result. One explanation for this discrepancy is the neglect of dissipative forces in calculating the desorption rates. The lowest-energy resonances of the surface reaction mechanism were tunneling states. The tunneling barrier is not coupled directly to the metal phonons. This precludes a phonon-assisted tunneling mechanism which was important in the hydrogen resurfacing dynamics. The role of phonons is therefore limited to hindering the desorption reaction rate. Another source of inaccuracy is caused by the reduced dimensionality model (two degrees of freedom). Higher-dimensionality calculations yield larger activation energies and lower desorption rates.[23] A calculation including all the hydrogen degrees of freedom and lattice dynamics is beyond current computer capabilities.

The reaction of the subsurface hydrogen with a nearby surface hydrogen atom was modeled by an uncorrelated two-step mechanism. The first step is the resurfacing of the bulk atom. The second step is the reaction of the hot hydrogen atom with a neighboring thermalized atom. This neglect of correlation is a source for a large underestimation of the reaction rate, since tunneling is involved. Indeed, it was found that the reaction rate adopted from the surface desorption calculation could not explain the existence of the low-temperature TPD peak.

Emission of hydrogen from the bulk to the surface creates short-lived hot hydrogen atoms. This model, which explains the additional reactivity of of bulk hydrogen, is radically different from the steric model of Johnson, Daley, and Ceyer.[10] This model was used to explain the desorptive reaction of bulk H with adsorbed CH_3. For hydrogen recombination the steric model seems to be inappropriate. However, for other reactions, it is possible that a combination of steric and energetic effects are responsible for the special chemistry of bulk hydrogen in nickel.

ACKNOWLEDGMENTS

This research was partially supported by the German Israel Foundation, and also partially supported by the Israel Atomic Energy commission and the Israel Council for Higher Education. The Fritz Haber Research Center is supported by the Minerva Gesellschaft für die Forschung, GmbH München, FRG.

APPENDIX A: ESSENTIALS OF THE SURROGATE HAMILTONIAN METHOD

The dynamics under study is a multimode coupled system-bath entity. The bath dynamics and its coupling to the system have to be reduced to a tractable computational scheme. This task is achieved by constructing a representation of the coupled system which is systematically improved enabling a study of convergence characteristics. Once the representative wave function has been constructed, the dynamics is determined by the expansion of the evolution operator $\hat{\mathbf{U}}(t)=\exp(-i\hat{\mathbf{H}}t/\hbar)$ or the Green operator $\hat{\mathbf{G}}(E)=(E-\hat{\mathbf{H}})^{-1}$ in terms of a Chebychev polynomial series.[80,81] The propagation enables a direct extraction of observable information.

1. Representation of the coupled system

The system-bath representation is developed through the study of the total Hamiltonian. This Hamiltonian is partitioned into the primary system's bare Hamiltonian $\hat{\mathbf{H}}_\mathbf{s}$ and the bath Hamiltonian $\hat{\mathbf{H}}_\mathbf{B}$, together with an interaction term $\hat{\mathbf{H}}_{\rm int}$, leading to

$$\hat{\mathbf{H}}=\hat{\mathbf{H}}_\mathbf{s}+\hat{\mathbf{H}}_\mathbf{B}+\hat{\mathbf{H}}_{\rm int}. \tag{A1}$$

The primary system Hamiltonian has the form

$$\hat{\mathbf{H}}_\mathbf{s}=\hat{\mathbf{T}}+V_s(\hat{\mathbf{R}}), \tag{A2}$$

where $\hat{\mathbf{T}}=\hat{\mathbf{P}}^2/2M$ is the kinetic energy of the primary system, and V_s is an external potential which is a function of the system coordinates $\hat{\mathbf{R}}$. The bath Hamiltonian $\hat{\mathbf{H}}_\mathbf{B}$ is decomposed to an infinite sum of normal modes,

$$\hat{\mathbf{H}}_\mathbf{B}=\sum_j \epsilon_j \hat{\mathbf{b}}_\mathbf{j}^\dagger \hat{\mathbf{b}}_\mathbf{j}. \tag{A3}$$

The index j is a multidimensional index describing a complex bath of bosonic modes with energies ϵ_j. Finally, the interaction term is a multiplication of a dimensionless geometric function $f(\hat{\mathbf{R}})$ with a boson mode $\hat{\mathbf{b}}_\mathbf{j}^\dagger$ of potential coupling strength V_j,

$$\hat{\mathbf{H}}_{\rm int}=f(\hat{\mathbf{R}})\sum_j V_j(\hat{\mathbf{b}}_\mathbf{j}^\dagger+\hat{\mathbf{b}}_\mathbf{j}). \tag{A4}$$

The operators $\hat{\mathbf{b}}_\mathbf{j}^\dagger$ and $\hat{\mathbf{b}}_\mathbf{j}$ are boson-type creation and annihilation operators, obeying the commutation rules

$$[\hat{\mathbf{b}}_\mathbf{j},\hat{\mathbf{b}}_\mathbf{j'}^\dagger]=\delta_{\mathbf{j},\mathbf{j'}}\hat{\mathbf{1}}. \tag{A5}$$

Equations (A1)–(A4) serve as the starting point of the investigation, but further reduction is required since these equations are too involved to be treated directly. The goal is to assemble a Hamiltonian consisting of a finite number of bath modes, which faithfully represents the dynamics of the primary system under the influence of an infinite bath for a finite time.

This goal is achieved by transforming the infinite boson bath to a simplified finite bath. This is done by examining the Heisenberg equations of motion for the primary system,

$$\dot{\hat{\mathbf{R}}}=\hat{\mathbf{P}}/M,$$

$$\dot{\hat{\mathbf{P}}}=-\nabla V_s(\hat{\mathbf{R}})-\nabla f(\hat{\mathbf{R}})\left(\sum_j V_j\hat{\mathbf{b}}_\mathbf{j}^\dagger+\text{H.c.}\right). \tag{A6}$$

The bath enters these equations through the following bath operator:

$$\sum_j V_j\hat{\mathbf{b}}_\mathbf{j}^\dagger+\text{H.c.}=\int \sqrt{J(\epsilon)}\hat{\mathbf{B}}^\dagger(\epsilon)d\epsilon+\text{H.c.}, \tag{A7}$$

where a creation operator $\hat{\mathbf{B}}^\dagger(\epsilon)$ for an *interaction boson* is defined

$$\hat{\mathbf{B}}^\dagger(\epsilon)=\frac{1}{\sqrt{J(\epsilon)}}\sum_j V_j\hat{\mathbf{b}}_\mathbf{j}^\dagger\delta(\epsilon-\epsilon_j). \tag{A8}$$

Similar equations exist for the corresponding annihilation operators. In these equations, $J(\epsilon)$ are normalization factors defined by

$$J(\epsilon)=\sum_j |V_j|^2\delta(\epsilon_j-\epsilon). \tag{A9}$$

These are needed so that $\hat{\mathbf{B}}_\epsilon^\dagger$ and $\hat{\mathbf{B}}_\epsilon$ retain the boson commutation relations

$$[\hat{\mathbf{B}}_\epsilon,\hat{\mathbf{B}}_{\epsilon'}^\dagger]=\delta(\epsilon-\epsilon'). \tag{A10}$$

The Heisenberg equations of motion for the boson operators are obtained from the Hamiltonian of Eq. (A3) by commutation,

$$\dot{\hat{\mathbf{B}}}(\epsilon)=-i\epsilon\hat{\mathbf{B}}(\epsilon)-if(\hat{\mathbf{R}})\sqrt{J(\epsilon)},$$

$$\dot{\hat{\mathbf{R}}}=\hat{\mathbf{P}}/M, \tag{A11}$$

$$\dot{\hat{\mathbf{P}}}=-\nabla V_s(\hat{\mathbf{R}})-\nabla f(\hat{\mathbf{R}})\int \sqrt{J(\epsilon)}\hat{\mathbf{B}}^\dagger(\epsilon)d\epsilon+\text{H.c.}$$

The Hamiltonian which contains the dynamical information about these equations of motion is the surrogate Hamiltonian

$$\hat{\mathbf{H}}_{\text{surr}}=\hat{\mathbf{T}}+V_s(\hat{\mathbf{R}})+\int \epsilon\hat{\mathbf{B}}^\dagger(\epsilon)\hat{\mathbf{B}}(\epsilon)d\epsilon + f(\hat{\mathbf{R}})\int \sqrt{J(\epsilon)}\hat{\mathbf{B}}^\dagger(\epsilon)d\epsilon+\text{H.c.} \tag{A12}$$

The consequence is that the system bath is fully characterized by the normalizing function, often called the spectral density $J(\epsilon)$. A derivation using path-integral methods leads to the same conclusion.[32]

The existence of the spectral density points the way to a convergent method of sampling the bath by a finite number of modes. A finite bath of N oscillators is constructed by requiring a spectral density which resembles, and, in the limit of $N\to\infty$, converges to, the given spectral density of the full bath. The algorithm of sampling the boson bath assumes that the given spectral density function $J(\epsilon)$ is of finite support, so that there exists an interval of energies $[\epsilon_o,\epsilon_c]$ outside of which the density is zero. The interval is sampled by selecting N energy points: $\epsilon_0<\epsilon_1<\cdots<\epsilon_{N-1}$. For each energy boson creation $\hat{\mathbf{B}}_m^\dagger$ and annihilation $\hat{\mathbf{B}}_m$ operators are defined. The energy sampling specifies a density of states for the discrete bath $\rho(\epsilon_m)\approx(\epsilon_{m+1}-\epsilon_m)^{-1}$. In conjunction with the spectral density sampling, the density of states imposed determines an effective interaction through the relation

$$U_m=\sqrt{J(\epsilon_m)/\rho(\epsilon_m)}. \tag{A13}$$

The discrete surrogate Hamiltonian therefore takes the following form:

$$\hat{\mathbf{H}}=\hat{\mathbf{T}}+V_s(\hat{\mathbf{R}})+\sum_{m=0}^{N-1}\epsilon_m\hat{\mathbf{B}}_\mathbf{m}^\dagger\hat{\mathbf{B}}_\mathbf{m}+f(\hat{\mathbf{R}})\sum_{m=0}^{N-1}U_m\hat{\mathbf{B}}_\mathbf{m}^\dagger+\text{H.c.} \tag{A14}$$

This construction has the merit that as N increases and the sampling becomes refined, the dynamical observables converge.

2. Boson bath as a set of two-level systems

The basic assumption is that the bath temperature is low. An actual dynamical calculation of the system and of the effective boson bath starts by assuming that no single-mode oscillator is strongly excited. Therefore, each mode is represented by a two-level system (TLS), leading to a replacement of the Boson operators by TLS operators

$$\hat{\mathbf{b}}^\dagger\to\hat{\sigma}_+,$$

$$\hat{\mathbf{b}}\to\hat{\sigma}_-. \tag{A15}$$

Notice that the commutation relations also transform,

$$[\hat{\mathbf{b}},\hat{\mathbf{b}}^\dagger]=1\to[\hat{\sigma}_-,\hat{\sigma}_+]=1-2\hat{\mathbf{n}}, \tag{A16}$$

where $\hat{\mathbf{n}}=\hat{\mathbf{b}}^\dagger\hat{\mathbf{b}}\to\hat{\mathbf{n}}=\hat{\sigma}_+\hat{\sigma}_-$. Since $\langle\hat{\mathbf{n}}\rangle$ is 1 for an excited TLS and 0 otherwise, the violation of the commutation relations is small if none of the TLS's are highly excited.

The numerical implementation of the dynamics of a subsystem coupled to N two level systems is best understood by first following the special case of a one mode $N=1$ bath. In this case the wave function is represented as a two-component spinor

$$\Psi(R)=\begin{pmatrix}\phi_0(R)\\ \phi_1(R)\end{pmatrix}. \tag{A17}$$

The 0 component corresponds to spin-down, and the 1 component to spin-up. The functions $\phi_m(R)$ are defined on equally spaced grids, although other representation techniques are possible. The R-independent spin operators appearing in the Hamiltonian are represented as 2×2 matrices in the two-component vector space

$$\hat{\mathbf{b}}^\dagger=\begin{pmatrix}0&0\\1&0\end{pmatrix},\quad \hat{\mathbf{b}}=\begin{pmatrix}0&1\\0&0\end{pmatrix},\quad \hat{\mathbf{n}}=\hat{\mathbf{b}}^\dagger\hat{\mathbf{b}}=\begin{pmatrix}0&0\\0&1\end{pmatrix}. \tag{A18}$$

For the general N oscillator case, a wave function is represented as a spinor of 2^N components bit ordered. This means that the mth component represents a spin arrangement deter-

mined by the 1's (spin-up) and 0's (spin-down) in its binary representation. Each component $\phi_m(R)$ is defined on the equally spaced grid. The Fourier method[80,81] is used for the representation of the system operators.

The wave-function representation is designed to perform sums of spin operators efficiently. The algorithm for applying the number operator for the kth spin, $\hat{\mathbf{n}}_\mathbf{k}$, on the wave function Ψ, consists of multiplying the component ϕ_m by the kth bit of the binary representation of the integer m (0 or 1).

Application of the operator $\Sigma_j V_j(R)\hat{\mathbf{b}}_\mathbf{j}^\dagger$ is performed by using recursion. The recursion is understood by studying the structure of the matrix representation of the interaction operator, although this matrix is never actually computed or stored.

The recursive form of the matrix can be generally described as follows. The $2^N\times 2^N$ matrix $\mathcal{V}_N$ defined by

$$\mathcal{V}_N=\begin{pmatrix} \mathcal{V}_{N-1} & V_{N-1}\mathbf{1}_{N-2} \\ V_{N-1}^*\mathbf{1}_{N-2} & \mathcal{V}_{N-1} \end{pmatrix}. \tag{A19}$$

The definition is recursive, with $\mathbf{1}_m$ being the $2^m\times 2^m$ unit matrix and $\mathcal{V}_{N=0}=0$. The operator $\mathcal{V}_N$ consists of only diagonal operations, reducing the numerical effort to a quasilinear one ($M\log M$), in the number of spinor components ($M=2^N$).

3. System-bath dynamics

The primary system is represented by the Fourier method,[80–82] enabling multidimensional systems to be analyzed with no restriction on the potential shape. Extracting dynamical information on the system requires propagation of an initial wave function by applying the evolution operator

$$\Psi(t)=\hat{\mathbf{U}}(t)\Psi(0)=e^{-i\hat{\mathbf{H}}t/\hbar}\Psi(0). \tag{A20}$$

The time dependence of the expectation value of any operator is determined by

$$\langle\hat{\mathbf{A}}(t)\rangle=\langle\Psi(t)|\hat{\mathbf{A}}|\Psi(t)\rangle. \tag{A21}$$

The evolution operator or the Green's-function operator is expanded by a series of Chebychev polynomials $C_n(\hat{\mathbf{H}})$, where $\hat{\mathbf{H}}$ is the Hamiltonian operator linearly scaled and shifted so that its spectrum is in the range $\{-1,1\}$.[81,80] The expansion coefficients are functions of t for the evolution operator $\hat{\mathbf{U}}(t)$ or of E for the Greenian operator $\hat{\mathbf{G}}(E)$. The propagator technique is also used to construct the initial state for the calculation. Propagating in imaginary time leads eventually to the fully correlated ground state of the combined system-bath entity.[83] By employing a filter-diagonalization method,[84,8] other eigenstates can be extracted directly. Thermal observables are obtained by Boltzmann weighting the results from the individual calculations.

APPENDIX B: STATIC BARRIER MODEL

The static barrier model is based on the adiabatic separation between the fast hydrogen motion and the slow lattice motion. This leads to an ansate for the total eigenstate wave function,

$$\Psi(R,Z)=\sum_n \chi_n(R)\phi_n(Z;R). \tag{B1}$$

The tunneling eigenstates are calculated for every R configuration, by solving the one-dimensional tunneling

$$\hat{\mathbf{H}}(Z;R)\phi_n(Z;R)=[E_n(R)-iJ_n(R)/2]\phi_n(Z;R), \tag{B2}$$

where E_n is the energy of the tunneling state and J_n is its tunneling rate. In this equation R is treated as a parameter. For deep tunneling, it is assumed that the ϕ_n wave functions are orthonormal,

$$\langle\phi_n|\phi_m\rangle=\delta_{n,m}. \tag{B3}$$

These results are inserted into the total Schrödinger equation. Integration over the Z coordinate, neglecting the derivatives of $\phi_n(Z;R)$ with respect to R (the adiabatic approximation), leads to a Schrödinger equation for the heavy oscillator:

$$\left(\hat{\mathbf{T}}_R+\frac{1}{2}m_s\omega_s^2R^2\right)\chi_{n,m}(R)+[E_n(R)-iJ_n(R)/2]\chi_{n,m}(R) =\epsilon_{n,m}\chi_{n,m}(R). \tag{B4}$$

Here an index m was added to identify the various solutions of the heavy-oscillator wave equation. Since the coupling is localized on the potential barrier, one finds a very small dependence of E_n on R (only a minute part of $\phi_{n,m}$ is on the barrier); hence this dependence was neglected. These approximations lead to a simple product form for the total wave function

$$\Psi_{n,m}(R,Z)=\chi_n,m(R)\phi_n(Z;R), \tag{B5}$$

where the real part of the energy levels becomes

$$\epsilon_{n,m}=(\tfrac{1}{2}+m)\hbar\omega_s+E_n. \tag{B6}$$

The tunneling rate is given approximately by averaging the J_n over the total eigenstate:

$$J_{n,m}=\int|\chi_{n,m}(R)|^2J_n(R)dR. \tag{B7}$$

The thermal tunneling rate is obtained by Boltzmann averaging of $J_{n,m}$. The final result can be written as

$$J(T)=\int P(R,T)J(R,T)dR, \tag{B8}$$

where $P(R,T)=e^{-R^2/2\sigma^2}/\sqrt{2\pi}\sigma$ is the thermal position distribution function of the heavy oscillator with $\sigma^2=(\hbar/2m_s\omega_s)\coth(\hbar\omega/2k_BT)$, the variance of a thermalized harmonic oscillator; and $J(R,T)=z^{-1}\Sigma_n e^{-\beta E_n}J_n(R)$ is the adiabatic thermal tunneling rate for a given position R of the heavy oscillator, where $z=\Sigma_n\exp(-\beta E_n)$ and $\beta=(k_BT)^{-1}$.

This expression was obtained using two basic assumptions. The first is the adiabatic approximation, while the second is the neglect of the dependence R.

APPENDIX C: SPECTRAL DENSITIES FROM MD SIMULATIONS

The results of MD calculations serve as a basis for quantum dynamical modeling of the resurfacing rates. This link is made through the concept of spectral density.

In the surrogate Hamiltonian method the interaction with the lattice phonons is determined by letting the lattice execute a classical MD motion, and monitoring the variation in the hydrogen potential during as a function of time. The following general form for the Hamiltonian of the few multimode baths can be written as:

$$\hat{\mathbf{H}}=\hat{\mathbf{T}}+\hat{\mathbf{V}}_{\mathbf{s}}(Z)+\sum_{i,k}\ (p^2/2m_{i,k}+m_{i,k}\omega_{i,k}^2x_{i,k}^2/2)$$

$$+\sum_i\ f_i(Z)\sum_k\ C_{i,k}x_{i,k}, \tag{C1}$$

where the connection with Eq. (6.1) is through the relations $V_{i,k}=C_{i,k}/\sqrt{2m_{i,k}\omega_{i,k}}$ and $\epsilon_{i,k}=\hbar\omega_{i,k}$. The functions $f_i(Z)$ are dimensionless functions of the hydrogen position. The spectral density is given by Eqs. (6.2) and (6.4). The total spectral density is determined by the molecular-dynamics simulation of the free crystal motion at a low temperature T. At every time step, the potential $V(t,Z_l)$ of the hydrogen atom is determined for a series of locations Z_l along the reaction coordinate,

$$\Delta(t,Z_l)=V(t,Z_l)-V_s(Z_l), \tag{C2}$$

where V_s is the adiabatic potential for the hydrogen motion. Under the composite bath model the recorded function is

$$\Delta(t,Z_l)=\sum_i\ f_i(Z_l)\sum_k\ C_{i,k}x_{i,k}. \tag{C3}$$

The analysis is based on the Wiener-Khinchin theorem. The finite Fourier transform of the difference function is defined by

$$U(T_f,\omega,Z_l)=\int_0^{T_f}\Delta(t,Z_l)e^{i\omega t}dt, \tag{C4}$$

where, T_f is the simulation time, chosen to be long enough. The Fourier transform of the autocorrelation function $C_\Delta=\langle\Delta(t,Z_l)\Delta(0,Z_l)\rangle=T_f^{-1}\int_0^{T_f}\Delta(t+\tau,Z_l)\Delta(\tau,Z_l)d\tau$ becomes

$$C_\Delta(T_f,\omega,Z_l)=(1/T_f)\int_0^{T_f}dte^{i\omega t}\int_0^{T_f}d\tau\Delta(\tau,Z_l)\Delta(t+\tau,Z_l)$$

$$=|U(T_f,\omega,Z_l)|^2/T_f. \tag{C5}$$

On the other hand, the Fourier transform of the autocorrelation $C_\Delta(\omega,T,Z_l)$ is directly related to the sums of spectral density functions, as shown by analyzing the autocorrelation function of the harmonic oscillator,

$$C_\Delta(t,Z_l)=\sum_i\ |f_i(Z_l)|^2\sum_k\ |Ci_k|^2\langle x_{i_k}^2\rangle\cos(\omega_{i,k}t)$$

$$=\sum_i\ |f_i(Z_l)|^2\sum_k\ \frac{\hbar|C_{i,k}|^2}{2m_{i,k}\omega_{i,k}}\coth(\beta\hbar\omega_{i,k}/2)$$

$$\times\cos(\omega_{i,k}t), \tag{C6}$$

where the quantum-mechanical expression was used for the autocorrelation function of the harmonic oscillator in thermal equilibrium at the inverse temperature β. The Fourier transform of this expression (for large T_f) is then connected with the sum of spectral densities

$$C_\Delta(T_f,\omega,Z_l)=\pi\hbar\coth(\beta\hbar\omega/2)\sum_i\ |f_i(Z_l)|^2J_i(\hbar\omega)$$

$$\times\lim_{T_f\to\infty}\frac{|U(T_f,\omega,Z_l)|^2}{\pi\hbar T_f}\tanh(\beta\hbar\omega/2). \tag{C7}$$

The sum of spectral densities obtained this way is shown in Fig. 18 for some of the chosen Z_l values.

[1] A. V. Hamza and R. J. Madix, J. Chem. Phys. **89**, 5381 (1985).
[2] A. D. Johnson, K. J. Maynard, S. P. Daley, Q. Y. Yang, and S. T. Ceyer, Phys. Rev. Lett. **67**, 927 (1991).
[3] Th. Kammler, S. Wehner, and J. Kuppers, Surf. Sci. **125**, 339 (1995).
[4] T.-S. Lin and R. Gomer, Surf. Sci. **255**, 41 (1991).
[5] X. D. Zhu, A. Lee, A. Wong, and U. Linke, Phys. Rev. Lett. **68**, 1862 (1992).
[6] A. Lee, X. O. Zhu, L. Deng, and U. Linke, Phys. Rev. B **46**, 15 472 (1992).
[7] S. E. Wonchoba, W. P. Hu, and D.G. Truhlar, Phys. Rev. B **51**, 9985 (1995).
[8] R. Baer, Y. Zeiri, and R. Kosloff, Phys. Rev. B **54**, R5287 (1996).
[9] M. J. Maynard, A. D. Johnson, S. P. Daley, and S. T. Ceyer, Faraday Discuss. Chem. Soc. **91**, 437 (1991).
[10] A. U. A. D. Johnson, S. P. Daley, and S. T. Ceyer, Science **257**, 223 (1992).
[11] J. Sheng and J. Z. H. Zhang, J. Chem. Phys. **96**, 3866 (1992).
[12] R. C. Mowrey, J. Chem. Phys. **99**, 7049 (1993).
[13] G. Comsa, J. Chem. Phys. **48**, 3235 (1968).
[14] H. S. R. L. Palmer, J. N. Smith, Jr., and D. R. O'Keefe, J. Chem. Phys. **53**, 1666 (1970).
[15] M. B. M. J. Cardillo and R. E. Stickney, Surf. Sci. **50**, 263 (1975).
[16] G. Comsa and R. David, Surf. Sci. Rep. **5**, 145 (1985).
[17] D. J. A. C. T. Rettner, H. A. Michelsen, and C. B. Mullins, J. Chem. Phys. **94**, 7499 (1991).
[18] H. A. Michelsen and D. Auerbach, J. Chem. Phys. **94**, 7501 (1991).
[19] H. A. Michelsen, C. T. Rettner, and D. J. Auerbach, in *Surface Reactions*, edited by R. J. Madix (Springer-Verlag, Berlin, 1993).

[20] C. T. Rettner, D. J. Auerbach, and H. A. Michelsen, Phys. Rev. Lett. **68**, 1164 (1992).
[21] G. R. Darling and S. Holloway, J. Chem. Phys. **101**, 3268 (1994).
[22] A. Gross, J. Chem. Phys. **102**, 5045 (1995).
[23] A. Gross, S. Wilke, and M. Scheffler, Phys. Rev. Lett. **75**, 2718 (1995).
[24] K. Yang and H. Rabitz, J. Chem. Phys. **101**, 8205 (1994).
[25] M. Persson and B. Hellsing, Phys. Rev. Lett. **49**, 662 (1982).
[26] B. Hellsing and M. Persson, Phys. Scr. **29**, 360 (1984).
[27] M. Head-Gordon and J. C. Tully, Phys. Rev. B **46**, 1853 (1992).
[28] M. Head-Gordon and J. C. Tully, J. Chem. Phys. **96**, 3939 (1992).
[29] T. N. Truong and D. G. Truhlar, J. Phys. Chem. **91**, 6229 (1987).
[30] S. E. Wonchoba and D. G. Truhlar, Phys. Rev. B **53**, 11 222 (1996).
[31] M. A. Collins, Adv. Chem. Phys. **93**, 386 (1996).
[32] A. J. Leggett, S. Chakravarty, A. T. Dorsey, M. P. A. Fisher, A. Garg, and W. Zwerger, Rev. Mod. Phys. **59**, 1 (1987).
[33] M. Topaler and N. Makri, J. Chem. Phys. **101**, 7500 (1994).
[34] C. H. Mak and R. Egger, Adv. Chem. Phys. **93**, 39 (1996).
[35] M. J. Gillan, J. Phys. C **20**, 3621 (1987).
[36] D. C. G. A. Voth and W. H. Miller, J. Phys. Chem. **93**, 7009 (1989).
[37] G. A. Voth, Adv. Chem. Phys. **93**, 135 (1996).
[38] Y. Li and G. Wahnstrom, Phys. Rev. Lett. **68**, 3444 (1992).
[39] Y. Li and G. Wahnstrom, Phys. Rev. B **46**, 14 528 (1992).
[40] T. R. Mattsson, U. Engberg, and G. Wahnstrom, Phys. Rev. Lett. **71**, 2615 (1993).
[41] T. R. Mattsson and G. Wahnstrom, Phys. Rev. B **51**, 1885 (1995).
[42] Y. Li and G. Wahnstrom, Phys. Rev. B **51**, 12 233 (1995).
[43] B. Whaley, A. Nitzan, and R. B. Gerber, in *Tunneling*, edited by J. Jortner and B. Pullman (Reidel, Dordrecht, 1986), p. 297.
[44] K. B. Whaley, A. Nitzan, and R. B. Gerber, J. Chem. Phys. **84**, 5181 (1986).
[45] M. J. Puska, R. M. Nieminen, M. Manninen, B. Chakraborty, S. Holloway, and J. K. Norskov, Phys. Rev. Lett. **51**, 1081 (1983).
[46] H. Grabert, in *Quantum Aspects of Molecular Motion in Solids*, edited by A. Heidemann, A. Magerl, M. Prager, D. Richter, and T. Springer (Springer-Verlag, Berlin, 1987), p. 130.
[47] K. F. F. A. Auerbach and R. Gomer, J. Chem. Phys. **86**, 2356 (1987).
[48] J. C. Tully, J. Chem. Phys. **73**, 1975,6333 (1980).
[49] N. E. Henriksen, G. D. Billing, and F. Y. Hansen, Surf. Sci. **227**, 224 (1990).
[50] H. Schlichting, D. Menzel, T. Brunner, W. Brenig, and J. C. Tully, Phys. Rev. Lett. **60**, 2515 (1988).
[51] E. K. Schweizer and C. T. Rettner, Phys. Rev. Lett. **62**, 3085 (1989).
[52] B. Jackson, J. Chem. Phys. **94**, 5126 (1991).
[53] B. Jackson, J. Chem. Phys. **90**, 1458 (1989).
[54] R. Kosloff and C. Cerjan, J. Chem. Phys. **81**, 3722 (1984).
[55] C. Cerjan and R. Kosloff, Phys. Rev. B **34**, 3832 (1986).
[56] G. D. Billing, Comput. Phys. Rep. **12**, 383 (1990).
[57] M. D. Stiles, J. W. Wilkins, and M. Persson, Phys. Rev. B **34**, 4490 (1986).
[58] B. Jackson, Comput. Phys. Commun. **80**, 119 (1994).
[59] C. T. Ceyer (private communication).
[60] M. S. Daw and M. I. Baskes, Phys. Rev. B **29**, 6443 (1984).
[61] R. Baer and R. Kosloff, J. Chem. Phys. (to be published).
[62] *Density Functional Theory of Many-Fermion Systems*, edited by S. B. Trikey (Academic, New York, 1990), Vol. 21.
[63] T. N. Truony, D. G. Truhlar, and B. C. Garrett, J. Phys. Chem. **93**, 8227 (1989).
[64] S. A. Adelman and B. J. Garrison, J. Chem. Phys. **65**, 3751 (1976).
[65] S. A. Adelman, Adv. Chem. Phys. **53**, 61 (1983).
[66] R. R. Lucchese and J. C. Tully, J. Chem. Phys. **61**, 6313 (1984).
[67] Y. Zeiri J. J. Low, and W. A. Goddard, J. Chem. Phys. **84**, 2408 (1986).
[68] D. Beeman, J. Comput. Phys. **20**, 130 (1976).
[69] E. Fermi and E. Teller, Phys. Rev. **72**, 399 (1947).
[70] T. L. Ferrell and R. H. Ritchie, Phys. Rev. B **16**, 115 (1977).
[71] R. A. Marcus, J. Chem. Phys. **45**, 4493 (1966).
[72] R. E. Wyatt, J. Chem. Phys. **51**, 3489 (1969).
[73] D. G. Truhlar, J. Chem. Phys. **53**, 2041 (1970).
[74] W. H. Miller, in *Tunneling*, edited by J. Jortner and B. Pullman (Reidel, Dordrecht, 1986), p. 91.
[75] W. H. Miller, in *The Theory of Chemical Reaction Dynamics*, edited by D. C. Clary (Reidel, Boston, 1986), p. 27.
[76] J. Kondo, Physica **125B**, 279 (1984).
[77] J. Kondo, Physica **126B**, 377 (1984).
[78] W. W. G. Eilmsteiner and A. Winkler, Surf. Sci. **352**, 263 (1996).
[79] O. Citri, R. Baer, and R. Kosloff, Surf. Sci. **351**, 24 (1996).
[80] R. Kosloff, J. Phys. Chem. **92**, 2087 (1988).
[81] R. Kosloff, in *Numerical Grid Methods and Their Application to Schrodinger's Equation*, edited by C. Cerjan (Kluwer, Dordrecht, 1993), p. 175.
[82] R. Kosloff, Ann. Rev. Phys. Chem. **45**, 145 (1994).
[83] R. Kosloff and H. Tal-Ezer, Chem. Phys. Lett. **127**, 223 (1986).
[84] Michael R. Wall and Daniel Neuhauser, J. Chem. Phys. **102**, 8011 (1995).